Alma Mater Studiorum · Università di Bologna

Scuola di Scienze

Corso di Laurea Magistrale in Fisica

Modelling the stable, nocturnal boundary layer: different approaches to turbulence closure problem

Relatore:

Prof. Francesco Tampieri

Presentata da:

Gabriele Arduini

Correlatore:

Prof. Chantal Staquet
Dott. Alberto Maurizi

Sessione I

Anno Accademico 2012/2013

Contents

List of Figures

List of Tables

Sommario

Il lavoro è dedicato all'analisi fisica e alla modellizzazione dello strato limite atmosferico in condizioni stabili. L'obiettivo principale è quello di migliorare i modelli di parametrizzazione della turbulenza attualmente utilizzati dai modelli meteorologici a grande scala. Questi modelli di parametrizzazione della turbolenza consistono nell' esprimere gli stress di Reynolds come funzioni dei campi medi (componenti orizzontali della velocità e temperatura potenziale) usando delle chiusure. La maggior parte delle chiusure sono state sviluppate per i casi quasi-neutrali, e la difficoltà è trattare l'effetto della stabilità in modo rigoroso. Studieremo in dettaglio due differenti modelli di chiusura della turbolenza per lo strato limite stabile basati su assunzioni diverse: uno schema TKE-l (Mellor-Yamada,1982), che è usato nel modello di previsione BOLAM (Bologna Limited Area Model), e uno schema sviluppato recentemente da Mauritsen et al. (2007). Le assunzioni delle chiusure dei due schemi sono analizzate con dati sperimentali provenienti dalla torre di Cabauw in Olanda e dal sito CIBA in Spagna. Questi schemi di parametrizzazione della turbolenza sono quindi inseriti all'interno di un modello colonnare dello strato limite atmosferico, per testare le loro predizioni senza influenze esterne. Il confronto tra i differenti schemi è effettuato su un caso ben documentato in letteratura, il "GABLS1". Per confermare la validità delle predizioni, un dataset tridimensionale è creato simulando lo stesso caso GABLS1 con una Large Eddy Simulation. ARPS (Advanced Regional Prediction System) è stato usato per questo scopo. La stratificazione stabile vincola il passo di griglia, poichè la LES deve essere ad una risoluzione abbastanza elevata affinchè le tipiche scale verticali di moto siano correttamente risolte. Il confronto di questo dataset tridimensionale con le predizioni degli schemi turbolenti permettono di proporre un insieme di nuove chiusure atte a migliorare il modello di turbolenza di BOLAM. Il lavoro è stato compiuto all' ISAC-CNR di Bologna e al LEGI di Grenoble.

Abstract

The work is devoted to the physical analysis and modelling of the stable atmospheric boundary layer. Our aim is to improve turbulence models currently implemented in weather forecast models. These turbulence models consist in expressing the Reynolds stresses as a function of the mean fields (horizontal velocity components and potential temperature), using closure assumptions. Most closure assumptions have been developed in the quasi-neutral case and the difficulty is to deal with the effects of stable stratification in a rigorous way. We shall analyze in detail two different turbulence models regarding the stable atmospheric boundary layer, based on different assumptions: the so-called TKE-l scheme (Mellor-Yamada,1982), which is used in the BOLAM (Bologna Limited Area Model) forecast model, and a scheme recently developed by Mauritsen et al. (2007). The closure assumptions of the two schemes are tested against experimental measurements from Cabauw tower in the Netherlands and from CIBA site in Spain. These turbulence schemes are then included in a Single Column Model (SCM) of the atmospheric boundary layer to test their predictions without any other influence. The comparison is made on the test- case "GABLS1", which is well-documented in the literature. In order to assess the validity of these predictions, a three-dimensional dataset shall be developed using a Large Eddy Simulations (LES) of the GABLS1 test-case. The ARPS (Advanced Regional Prediction System) code shall be used for this purpose. The stable stratification constrains the grid size so that the LES should be of high enough resolution for the typical vertical scale of the motion to be properly solved. Comparison of this dataset with the predictions of the turbulence models allows us to propose a set of new closure assumptions which improves the BOLAM turbulence model. The master's work has been carried out at the ISAC-CNR of Bologna and at LEGI in Grenoble.

"Scegli il lavoro che ami e non lavorerai mai, neanche per un giorno in tutta la tua vita"

Dedicato a chi mi permette di provarci.

E un po' anche a me, che ci provo.

1 Introduction

1.1 A very short introduction

In the last page of his second book of *lectures on physics* devoted to hydrodynamic and turbulence, Richard Feynman wrote (Feynman et al., 1969, chapter 21):

> *" Often, people in some unjustified fear of physics say you can't write an equation for life. Well, perhaps we can. As a matter of fact, we very possibly already have the equation to a sufficient approximation when we write the equation of quantum mechanics "*:
>
> $$H\phi = +i\hbar\frac{\partial}{\partial t}\phi$$

Of course, the Feynman's sentence is a clear hyperbole. What he would like to express is that the complexity of nature is easily hidden behind the elegant form of the equations which we use to represent it. In a provocatory fashion, Richard Feynman suggests that although we can write an equation for a class of phenomenons, we are still not able to catch all the qualitative behaviours that such equation should explain. Having only the Heisenberg's equation, we would be unable to reconstruct all the world around us.
Feynman believes that an analogous situation prevails in turbulent flows of an incompressibile fluid: we may already write an equation that perhaps contains everything about turbulence:

$$\frac{\partial}{\partial t}\vec{v} + (\vec{v}\cdot\nabla)\vec{v} = -\frac{1}{\rho}\nabla p + \nu\nabla^2\vec{v} + F_{ext}\ , \tag{1}$$

$$\nabla\vec{v} = 0$$

that it is the well-known (at least since Navier) Navier-Stokes equations. If completed with initial and boundary conditions, it could describe all flow motions which can develop in such particular situation (the situation described by those initial and boundary conditions). As for the clear quantum mechanics example, the problem is more complicated (otherwise this dissertation would be completely irrelevant): following Feynman's

argument, we are still unable to get the infinite qualitative behaviours of nature from the couple of equations (1), even though they are *within* them. Of course they are well hidden by mathematical issues, but clearly inside the equations. To reveal them distinctly, we need experiments, that give us a set of concepts and approximations that enable us to discuss the potential hidden solutions of equations.
Atmospheric boundary layer flows are potentially described by a set of already well-known equations. But nothing can be said without attempts, hypothesis, approximations.
The case of stably stratified atmospheric flows is difficult to tackle, since together with theoretical issues, we must deal with experimental issues: the quantities that must be measured are small, and in very stable conditions (the definition of "very stable condition" will be given later) they can be less than instrumental resolution. Therefore it is necessary to deal with the problem using numerical simulations.

1.2 From Navier Stokes equation to RANS equation

Although we are able to write the differential equation governing the motion, hence to know a possible deterministic solution of, i.e. the time evolution of the wind, the exact solution (analytical and even numerical) is not computable:
It is well-known (since Reynolds, 1883) that turbulent motions develop inside a flow at high Reynolds numbers, making impredictable the exact motion of the flow. All the quantities are characterized by casual fluctuations, related to the interactions of nonlinear inertia terms (which dominate at high Reynolds numbers) in the equations of motion.
A qualitative picture of where the impredictability come out is explained by Vallis (2006) in terms of *triad interactions*: let's assume the equation (1) without pressure terms and viscous terms. The latter semplification is also reasonable for high Reynolds numbers flows, because for such flows the viscous contribution is negligible compared to the other terms ($Re >> 1$ the flow is almost inviscid (Landau and Lifshitz, 1987)). We shall assume for simplicity the horizontal component of the flow u, indipendent from x, y, hence $u \equiv u(z,t)$. If we suppose that the flow is confined in a square domain with periodic boundaries, we can expand $u(z)$ in Fourier series so that:

$$u(z,t) = \sum_{k_z} \tilde{u}_{k_z}(t) e^{ik_z z} \qquad w(x,y,z,t) = \sum_{\vec{k}} \tilde{w}_{\vec{k}}(t) e^{i\vec{k}\vec{x}} \tag{2}$$

by substituting it in the simplified (1), multiplying by $e^{-ik_z z}$ and integrating over the domain, we can find a time evolution equation for the Fourier coefficients $\tilde{u}_k(t)$:

$$\frac{\partial}{\partial t}\tilde{u}_k(t) = -\sum_{\vec{p},\vec{q}} A(\vec{p},\vec{q},\vec{k})\tilde{w}(\vec{p},t)\tilde{u}(\vec{q},t) \qquad A(\vec{p},\vec{q},\vec{k}) = q_z\delta(\vec{p}+\vec{q}-\vec{k}) \tag{3}$$

with $\vec{k} \equiv (0,0,k_z)$, $\vec{q} \equiv (0,0,q_z)$. $A(\vec{p},\vec{q},\vec{k})$ is an interaction coefficient, and should be pointed out that only those wavevectors with $\vec{p}+\vec{q}=\vec{k}$ make a non zero contribution, thanks to the Dirac's delta function.

If we now consider at the initial time only two excited Fourier modes, corresponding to wavenumber $\vec{p},\vec{q}$ (together with their conjugate symmetric $-\vec{p},-\vec{q}$), then, these modes interact obeying to eq.(3) to generate a third and fourth wavenumber $\vec{k}=\vec{p}+\vec{q}$, $\vec{m}=-\vec{p}-\vec{q}$. These wavenumbers may interact with each other, exciting new fourier modes, $\vec{k}+\vec{p}$, $\vec{k}+\vec{m}$ *etcetc.* This process may excite in small time all the spectrum, producing the casual fluctuations observed in the flow. Moreover, let us consider two flows with very close, but not equal, initial conditions: they may be thought as flows with different excited Fourier modes at the initial time. Then the process described above may lead to completely different realizations of the flows after little time (sensitivity to initial conditions). It is important to note that this interaction is fully due to the non linear nature of equation (1).

Looking at experimental realizations of flows at high Reynolds number, the question is even more interesting: figure 1 represents the sampling in time of the axial component of a turbulent jet (Pope, 2000). Despite the randomness of the motions, due to the non-linear interactions between scales, the turbulent flow have clear statistical properties such us a mean value (depicted with a straight line in figure 1), along which the flow fluctuates. It is important to observe that the sample exhibits variations on a wide range of timescales.

The impredictable motion of the fluid, the presence of fluctuations at every scale of motion, and the presence of statistical properties that appear to restore a symmetry in the flow (in a statistical sense), are all properties of the so-called *fully developed turbulence.* All these properties are common to all fluids at very high Reynolds number ($Re > 1000$) (Frisch, 1995). In this framework, a probabilistic description of turbulence is straightforward and it is exactly what we are going to do.

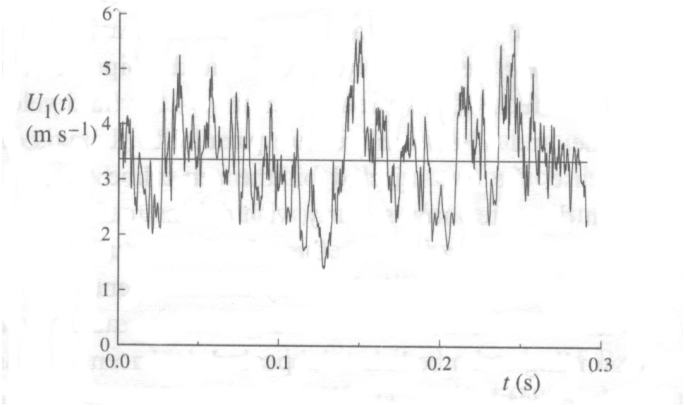

Figure 1: Time sampling of the axial component of velocity ($U_1(t) \equiv U(x,t)$) on the centerline of a turbulent jet. (from Pope, 2000).

1.2.1 The concept of Reynolds decomposition and average

What it is usually done is the decomposition of the fields in what is called a Reynolds decomposition:

$$\phi(x,y,z,t) = \bar{\phi}(x,y,z,t) + \phi'(x,y,z,t) \tag{4}$$

Without entering in details (which is far beyond the scope of this work), $\bar{\phi}(x,y,z,t)$ represents the first moment of the *random field* ϕ. With random field we intend (Monin and Yaglom, 1971, pag.211) a field for which exists a statistical ensemble of similar fields, called realizations. This ensemble of fields must have a definite probability density function (pdf) $p(\phi)$. Then the mean of the field ϕ is defined:

$$\bar{\phi} = \frac{1}{N}\int_{-\infty}^{+\infty} \phi p(\phi) d\phi \qquad N = \int_{-\infty}^{+\infty} p(\phi) d\phi \tag{5}$$

In this framework the concept of average is the probability average, or ensemble average. The statistical theory of turbulence that we use in this work is based on this concept.
In practical applications, i.e. atmospheric measurements, it is impossible to realize a set of similar flows: the "external conditions" are not fixed, hence we can not reproduce the same experiment, obtaining a different realization of the same flow. For experimental measurements, either time average or space average are used. The problem is shifted to look at how close the mean value, obtained with time-space average of a single experiment, lies to the ensemble mean value. In some particular cases, under strict conditions, the time - space average are equivalent to ensemble average (i.e. in a stationary field (see i.e. Monin and Yaglom, 1971)).

Recalling eq.(4), the "overbar" component is the mean part of the field "embedded" inside the total field ϕ. ϕ' is the fluctuation part which contains all the informations about the turbulent eddies at all scales of motion. That is, the turbulent motion is depicted as a superposition of "eddies" of different sizes. By the "size" of eddies, we mean the order of magnitude of the distances over which the velocity varies appreciably. As Re increases, large eddies appear first; the smaller eddies appear later. Hence, for a flow with very large Re eddies of every size are present from the largest to the smallest (Landau and Lifshitz, 1987).
The size of the largest eddies belongs to the order of the dimensions l of the region in which the flow takes place. In the atmospheric boundary layer for instance, l scales with the boundary layer depth (and define the "external " scale of turbulence (Landau and Lifshitz, 1987)). The velocity in them is comparable to the variation of the mean velocity over the distance l, saying Δu. These large eddies have the largest amplitude, thus they contain the major part of "turbulent kinetic energy" (the rigorous concept of turbulent kinetic energy will be explained in next chapter).
The small eddies may be regarded as a fine detailed structure superposed on the fundamental large turbulent eddies. Over small distances, compared to the external scale l, the variation of the fluctuating velocity is given by the variation in the velocity in these smallest eddies. This variation, say δu, is small compared to Δu, but at the same time it is large if compared to the variation of the mean velocity over these small distances (Landau and Lifshitz, 1987). So that is why in situations where the largest turbulent eddies are inhibited (like in strongly cooled clear air nights...) turbulence is still present,

acting in order to mix the fields. This mixing (due to the smallest eddies) is however faster and stronger than the mixing expected in a laminar flow.

Ensemble average (and hence even the time and spatial average in their particular cases) is a linear operation, so it respects the so-called *Reynolds average rules*. The most important properties of this kind of average are (see for details Monin and Yaglom, 1971):

$$\overline{\bar{\phi}} = \bar{\phi} \qquad \overline{\phi'} = 0 \ , \qquad \overline{\frac{\partial}{\partial s}\phi} = \frac{\partial}{\partial s}\bar{\phi}$$

That is: the mean of the mean part does not change anything, the mean of the fluctuations is zero, and the averaging operation commutes with linear operators. In the main part of this work with $\overline{[\cdot]}$ symbol we shall consider ensemble average.

1.2.2 Application to Navier-Stokes equations

In this work I would rather use, when it is possible, Einstein's notation to write the equations. Applying the Reynolds decomposition at the mass conservation equation (the second of eq.(1)), we first obtain:

$$\frac{\partial}{\partial x_i}\bar{u}_i = 0 \qquad \frac{\partial}{\partial x_i}u_i' = 0 \tag{6}$$

This states that the incompressibility condition is satisfied for both the mean part and the fluctuating part of the flow. Bearing this in mind and applying the same decomposition to the first of (1), we shall obtain the so-called Reynolds Average Navier-Stokes equations (RANS):

$$\frac{\partial}{\partial t}\bar{u}_i + \left(\bar{u}_j\frac{\partial}{\partial x_j}\right)\bar{u}_i = -\frac{1}{\rho}\frac{\partial}{\partial x_i}\bar{p} + \nu\frac{\partial^2}{\partial x_j \partial x_j}\bar{u}_j - \frac{\partial}{\partial x_j}\overline{u_i' u_j'} \tag{7}$$

If we compare equation (7) with equation (1) we find a new "extra" term on the rhs of equation (7): this term comes out from the non-linear advection term. In facts, if we apply Reynolds decomposition to the second term in lhs of equation (1), using incompressibility condition (6) it is straightforward to see:

$$(\bar{u}_j + u'_j)\frac{\partial}{\partial x_j}(\bar{u}_i + u'_i) = \bar{u}_j\frac{\partial}{\partial x_j}\bar{u}_i + \frac{\partial}{\partial x_j}\overline{u'_j u'_i} \tag{8}$$

We cannot evaluate the last term in the rhs of the equation (8) only by the knowledge of the mean part $\bar{u}$, because it requires the knowledge of the correlation of the fluctuating part of the flow. If we try to find an equation governing this *second order* term, we find the same problem, with a third order term and so on. This problem is called the *closure* problem of turbulence.
The correlation term, called *Reynolds stress*, is the interaction term between mean field and fluctuations: it represents the effect of eddies to the mean flow. It should be pointed out that with Reynolds decomposition and average, this term contains the information about eddies of *all* scales, from the smallest, to the biggest.
Considering the density mass in equation (7), we may write the Reynolds stresses:

$$\rho\overline{u'_j u'_i} = \overline{u'_j m'_i} \tag{9}$$

where $m'_i \equiv \rho u'_i$ is the fluctuating momentum. Then the Reynolds stress term (9) may be interpreted as the flux along j-direction, due to fluctuating velocity u'_j, of the momentum m'_i . Interpreted as a flux, it is easy to understand that the term (9) acts in order to enhance the mixing of the component $\bar{u}_i$, in addition to the molecular diffusion.

The problem of turbulence modelling may be easily summarized by equation (8): "We need a representation of Reynolds stresses in terms of the mean quantities". At this time, the only way to do that is to introduce physical assumptions which are not direct consequence of the equations. These assumptions link together mean flow and correlations, enabling to solve the problem, to *close* the equations. The set of assumptions and corresponding equations forms a *closure scheme* of Reynolds averaged equations.

In this work we study different closure schemes developed for turbulence modellization in weather forecast models based on RANS. In chapter 2 we write the set of equations characterizing atmospheric turbulence, which we are going to use in the rest of the work. In particular, we focus on atmospheric turbulence in a stably stratified atmosphere, which is described in chapter 3. A deep insight on different schemes is done in chapter

4, dedicated to the parametrization of the Reynolds stresses.
The analyzed schemes are tested in a highly simplified numerical model of the atmosphere presented in chapter 5, and they are compared to each other in chapter 6 using a three-dimensional numerical simulation.

2 Governing equations of atmospheric turbulence

In this chapter we shall introduce the set of equations confining the problem to atmospheric turbulence, and, in particular, to turbulence in atmospheric boundary layer.

In order to simplify the problem, we shall not take into account the contribution of water vapor: we shall consider a dry atmosphere.
With this initial approximation, the set of governing equation does not include an equation for time evolution of water vapor, and we shall not consider the variation of temperature due to water vapor contribution (virtual temperature is equal to absolute temperature, $T_v = T$).
The second basic approximation, is the Boussinesq approximation: the termodynamic variation of the properties of fluid are neglected (see i.e. Spiegel and Veronis, 1960), apart the density differences associated with the force of gravity (buoyancy).

2.1 The equations of the mean fields

The set of equations is composed by a set of conservation laws (plus an equation of state for gases):

Conservation of density mass, already written in (6), with the incompressible approximation that it is included in Boussinesq approximation.

Conservation of sensible heat per unit mass, that it is equivalent to write a conservation equation for temperature, if the specific heat at costant pressure c_p is costant:

$$\frac{\partial}{\partial t}\theta + u_j \frac{\partial}{\partial x_j}\theta = \chi \frac{\partial^2}{\partial x_j^2}\theta + R \tag{10}$$

where we use potential temperature θ, the value of temperature purified of adiabatic contribution associated with the pressure variation used to bring the fluid at the reference atmospheric pressure. It is a very useful quantity because, by definition, it is conserved during an isoentropic motion. Hence, i.e. it allows us to neglect the adiabatic lapse rate when we think about vertical motions of fluid particle.

χ is the molecular thermal diffusivity and R represents radiative heat flux, or any other source term for heat. We do not write it explicitely because we are going to discard it as soon as possible.
If we apply again Reynolds decomposition and average, we obtain the equation for time evolution of mean temperature:

$$\frac{\partial}{\partial t}\bar{\theta} + \bar{u}_j \frac{\partial}{\partial x_j}\bar{\theta} = \chi \frac{\partial^2}{\partial x_j^2}\bar{\theta} + \bar{R} - \frac{\partial}{\partial x_j}\overline{u_j'\theta'} \tag{11}$$

where the Reynolds stress term compares on the rhs of the equation. Phisically, it has the same interpretation of Reynolds stresses of eq.(7): it represents the flux of heat due to the fluctuation velocity component u_j'.
Conservation of momentum, namely the Navier-Stokes equation:(1) must be modified in order to include all the body forces acting on an atmospheric flow: we need to add the gravity force and the effect of the rotation of earth, the Coriolis force. With these two extra forces equation (7) become:

$$\frac{\partial}{\partial t}\bar{u}_i + \left(\bar{u}_j \frac{\partial}{\partial x_j}\right)\bar{u}_i = +\delta_{i3} g \frac{\bar{\theta}}{\theta_0} + \epsilon_{ij3} f \bar{u}_j - \frac{1}{\rho_0}\frac{\partial}{\partial x_i}\bar{p} + \nu \frac{\partial^2}{\partial x_j \partial x_j}\bar{u}_i - \frac{\partial}{\partial x_j}\overline{u_i' u_j'} \tag{12}$$

where we have already written the pressure term without the hydrostatic contribution, so $\bar{\theta}$, in this case, represents the departure from the reference state θ_0. $+\delta_{i3} g \frac{\bar{\theta}}{\theta_0}$ is called buoyancy term and represents the force on an air parcel when it is colder or warmer than the surrounding: i.e. during the day solar radiation heats the ground, which transfers heat to the air above. Then this air at height z has a temperature θ heigher than surrounding air at base state temperature $\theta_0(z)$. According to eq.(12) the buoyancy term is positive, and then the air feels a positive acceleration, directed upward. Obviously the acceleration is directed downward if the air has a temperature lower than the reference state.

2.2 The equations of the second order moments

From this set of equations for the mean quantities we can calculate the evolution equations for the higher order moments.

The equations of correlation terms $\overline{u_i' u_j'}$ may be obtained by subtracting the equations for the mean flow to equations for "total" flow and then multiplying each other the equations for perturbations with different indeces (see i.e. Wyngaard, 2010). The equation for the Reynolds stresses (correlations between velocity components) is:

$$\frac{\partial}{\partial t}\overline{u_i' u_k'} + \bar{u}_j \frac{\partial}{\partial x_j}\overline{u_i' u_k'} = (T) + (Shear\ prod) + (buoyancy) + (Coriolis) + (Dissipation) \quad (13)$$

where each single term represents:

- $T = -\frac{\partial}{\partial x_j}\overline{u_i' u_j' u_k'} - \frac{1}{\rho_0}(\overline{u_k' \frac{\partial}{\partial x_i} p'} + \overline{u_i' \frac{\partial}{\partial x_k} p'})$: transport terms of the stresses. The first could be associated with a flux of the stresses, the second is the correlation between the fluctuations and the gradient of pressure fluctuations. They represent the third order terms that appear when we look for an equation for the second order terms.

- $Shear = -(\overline{u_i' u_j'} \frac{\partial}{\partial x_j}\bar{u}_k + \overline{u_k' u_j'} \frac{\partial}{\partial x_j}\bar{u}_i)$: it represents the production of turbulence due to shear. Even without any analysis, it is clear that the gradient of velocity components acts in order to enhance the turbulence inside a flow.

- $Buoyancy = +\frac{g}{\theta_0}(\delta_{k3}\overline{u_i'\theta'} + \delta_{i3}\overline{u_k'\theta'})$: it represents the contribution of gravity force. Unlike the shear-term that acts always to produce turbulence, buoyancy term is a bit more ambiguos: it could act in order to produce or to destroy the turbulence in a flow. We are going to analyze it in details in the next chapter.

- $Coriolis = +f(\epsilon_{kj3}\overline{u_i' u_j'} + \epsilon_{ij3}\overline{u_k' u_j'})$: it is the effect of Earth rotation on Reynolds stresses.

- $Dissipation = \nu(\frac{\partial^2}{\partial x_j^2}\overline{u_i' u_k'}) - 2\nu\overline{\frac{\partial}{\partial x_j}u_i' \frac{\partial}{\partial x_j}u_k'}$: it is the dissipation of Reynolds stresses. The first term corresponds to molecular diffusion, and at high Reynolds numbers it is negligible in confront to the second. The second term is the correlation between the *shear of fluctuations*: if we assume at the small dissipative scales homogeneus and isotropic turbulence, then the off-diagonal terms are zero and we can write this term $\nu\overline{(\frac{\partial}{\partial x_j}u_i')^2} \equiv \epsilon$. It is always positive and then with the minus sign in front it is a dissipative term: it represents the molecular destruction of the quantity $\overline{u_i' u_k'}$ and then the conversion of kinetic energy in internal energy.

If in the lhs of (13) the indeces are equal we obtain the time-evolution equation for the sum of variances of the velocity components (sum on repetead indeces).
This quantity is called the turbulent kinetic energy (TKE) $\frac{1}{2}\overline{u_i' u_i'} = \frac{1}{2}\overline{u'^2} + \frac{1}{2}\overline{v'^2} + \frac{1}{2}\overline{w'^2} \equiv E_k$:

$$\frac{d}{dt}E_k = -\overline{u_i' u_j'}\frac{\partial}{\partial x_j}\bar{u}_i - (T) + \frac{g}{\theta_0}\overline{w'\theta'} - \epsilon \tag{14}$$

where we have neglected the Coriolis and molecular diffusion terms, and written the substantial derivative on the lhs. It should be pointed that the equation (13) represents the complete matrix of time evolution of the Reynolds stresses, whereas (14) represents the trace of the time evolution tensor of Reynolds stresses, which in turn represents the interaction between mean flow and turbulent eddies: hence, (13) and (14) contain the sources, the sinks, and redistributions of turbulence in a flow. In particular, (14) represents the isotropic component of the time evolution Reynolds stresses tensor, and then it supplies *only* the production/dissipation of turbulence, without exchanging/redistribution terms (in analogy with deformations tensor where the trace represents the relative change of volume due to deformation).

Similar equations may be written for correlations and variance of scalar quantities, i.e. for the potential temperature:

$$\frac{d}{dt}\overline{u_i'\theta'} = (-\overline{u_i' u_j'}\frac{\partial}{\partial x_j}\bar{\theta} - \overline{u_j'\theta'}\frac{\partial}{\partial x_j}\bar{u}_i) - (T) + \delta_{i3}\frac{g}{\theta_0}\overline{\theta'^2} + \left(\overline{\nu\theta'\frac{\partial^2}{\partial x_j^2}u_i'} + \overline{\chi u_i'\frac{\partial^2}{\partial x_j^2}\theta'}\right) \tag{15}$$

$$\frac{1}{2}\frac{d}{dt}\overline{\theta'^2} = -\overline{u_i'\theta'}\frac{\partial}{\partial x_i}\bar{\theta} - \epsilon_\theta - (T) \tag{16}$$

where (T) represents again the third order terms due to the transport of the flux and the coupling of temperature fluctuations and pressure fluctuations.
It is possible to link the temperature variance with a "turbulent potential energy": the vertical displacement of a fluid particle leads to a variation of the potential energy associated with the fluid particle. In particular, if the displacement occur in a stratified fluid, at the first order the potential energy variation per unit mass associated is:

$$\delta E_P = \frac{1}{2}|N^2|\delta z^2 \tag{17}$$

The vertical variations δz are linked with temperature variations:

$$\delta z \frac{d\theta}{dz} = \delta\theta \tag{18}$$

Hence substituing (18) in (17) and averaging we have:

$$E_P = \frac{1}{2} \frac{\left(\frac{g}{\theta_0}\right)^2}{|N^2|} \overline{\theta'^2} \tag{19}$$

Hence, assuming that N^2 changes only slowly compared to the turbulent variations, multiplying eq.(16) by $\frac{(\frac{g}{\theta_0})^2}{|N^2|}$, we shall obtain an equation for the turbulent potential energy (TPE):

$$\frac{d}{dt}E_P = -\frac{g}{\theta_0}\overline{u_i'\theta'} sgn\left(\frac{d\theta}{dz}\right) - \epsilon_P - (T) \tag{20}$$

If the only important turbulent heat flux is the vertical flux $\overline{w'\theta'}$, we may observe that when potential temperature gradient is positive (potential temperature increases with height), buoyancy term appears with opposite signs in the budget equations of TKE and TPE. Hence, buoyancy term may be thought as a conversion term of turbulent kinetic energy in turbulent potential energy. Summing together TKE and TPE, an equation for the *total* turbulent energy (TTE) may be obtained:

$$\frac{d}{dt}E = -\overline{u_i'u_j'}\frac{\partial}{\partial x_j}\bar{u}_i - (T) - \epsilon_E \quad if \quad \frac{d\theta}{dz} > 0 \tag{21}$$

Otherwise, when potential temperature gradient is negative, the buoyancy terms in (14),(20) have concordant signs. Then, summing the two equations, the budget equation for total turbulent energy is:

$$\frac{d}{dt}E = -\overline{u_i'u_j'}\frac{\partial}{\partial x_j}\bar{u}_i + 2\frac{g}{\theta_0}\overline{w'\theta'} - (T) - \epsilon_E \quad if \quad \frac{d\theta}{dz} < 0 \tag{22}$$

2.3 The Single Column approximation

If we consider the mean velocity and temperature horizontally homogeneus and we consider motions only on a flat terrain, the equations of motion may be strongly simplified. The former condition permits to neglect the horizontal gradients of the advective term.

Hence, using the continuity equation (6) and the flat terrain hypothesis, it follows $\bar{w}(z) = 0$.
Typical (horizontal) scales of mean velocity are several orders less than typical pressure gradient scales ($L_u \sim 10^3 m << L_p \sim 10^6 m$). Hence, from the geostrophic balance

$$\frac{1}{\rho_0}\frac{\partial \bar{p}}{\partial x_i} = f\epsilon_{ij3}v_{gj} \tag{23}$$

may be inferred that there are not strong variations of the geostrophic wind over the distance L_u, and we may take it indipendent by horizontal coordinates. Moreover, if we assume that temperature is homogeneus over the same scale L_u, from thermal wind equation, we may assume the atmosphere barotropic and then consider the geostrophic wind costant with height as well.
In atmosphere Reynolds number is much larger than one, so we may neglect molecular viscous diffusion.
Taking into account these approximations, the equations of motion (10), (12) reduce to:

$$\frac{\partial \overline{u}(z)}{\partial t} = +f(\overline{v}(z) - v_g) - \frac{\partial \overline{u'w'}}{\partial z} \tag{24}$$

$$\frac{\partial \overline{v}(z)}{\partial t} = -f(\overline{u}(z) - u_g) - \frac{\partial \overline{u'w'}}{\partial z} \tag{25}$$

$$\frac{\partial \overline{\theta}(z)}{\partial t} = -\frac{\partial \overline{\theta'w'}}{\partial z} + R \tag{26}$$

The system of equations (24), (25), (26) is analogous to a one-dimensional model of the atmosphere, where the "horizontal contributions" to the evolution of motion are neglected.
Strictly speaking, it is equivalent to run a three-dimensional model on a single horizontal grid point: then the name "Single Colomn". In all the simulations we do not consider radiative effects and we substitute it with a simple ground cooling. This rough forcing model avoids the use of a model for the soil, assuming implicitly an energetic balance between the soil and the atmosphere above. Then, we do not take into account any coupling or feedback between ground and air, which are an important issues in stable boundary layer modelling (see i.e. the model of Costa et al., 2011).

3 The atmospheric Boundary Layer

Atmospheric boundary layer (ABL) could be defined as the part of the atmosphere directly influenced by the earth's surface (Garratt, 1992). By "influenced" we mean that the physics generated by the presence of the surface has an effect on the air above on a time scale which is less than a day.
It is quite straightforward that this kind of definition is far from being precise. Different kinds of surfaces may produce different kinds of turbulent fluxes, that modified the structure of the atmospheric flow, making it completely different from the flow in the free atmosphere. But, over the land, the behaviour of ABL is strongly influenced by diurnal cycle: solar influence on the sign of vertical heat fluxes permits to roughly divide the ABL in three main categories:

- $\overline{w'\theta'} = 0$: neutral boundary layer
- $\overline{w'\theta'} > 0$: convective (unstable) boundary layer
- $\overline{w'\theta'} < 0$: stable boundary layer

A truly neutral atmosphere is difficult to observe in the real world, since heat fluxes are always present.
Convective boundary layer is the situation that we observe during the day, when the ABL is dominated by the heating of the sun and the heat fluxes are positive (forming i.e. plumes and thermals).
Stable boundary layer, when heat fluxes are negative, is the central topic of this work and it will be discussed in the next sections.

3.1 The Stable Boundary Layer

Let's start from a figure:

Figure 2: Smoke of a fire is " blocked " due to stable stratification in Lunigiana fields, Massa-Carrara

Picture 2 was taken one hour after the sunrise in winter 2013, with clear sky during the night. In the figure, the signature of the stable stratification, still present at this time of the morning, is clearly visible: according to parcel theory, the warm "smoke parcels" are buoyancy forced to move upward. This upward motion lasts as long as the smoke is warmer than surrounding air. Then, when parcels are in thermal equilibrium with the sorrounding their motion is blocked. In a convective situation this easy picture is "distorted" by turbulent eddies, which quickly mix the smoke (and any other scalar) making it impossibile to recognize after a while.
In figure 2, on the other hand, there is not a clear signature of turbulent motions (at least of large scales). When the smoke reaches the equilibrium height with sorrounding, it is just "spread" by the wind (that it was very low) over the horizontal.
Regarding figure 2, we may already infer two main properties of the Stable Boundary Layers (SBLs):

- They are characterized by very low turbulent activity (no big-scale eddies).
- They are characteristic of nighttime, when solar short wave energy contribution is not present. During the day, solar heating is the main responsible of the formation of turbulent eddies, which could reach size comparable with the height of boundary layer.

In our great division of ABL, made in the previous paragraph we state that stable boundary layers are characterized by negative turbulent heat fluxes. Now we can explain that: when the day ends, after sunset, due to longwave emission the ground starts to cool in respect to the air above. Then we observe a situation called "inversion", when the temperature at surface is colder then the air above. In this situation temperature fluctuations θ' are always negatively correlated with vertical velocity fluctuations w'. The resulting fluxes are then negative as we wrote ((see i.e. Garratt, 1992) and directed downward.
To say that turbulence activity in stable conditions is small, is like saying that turbulent fluxes are small. Therefore if we assume that the absolute value of turbulent fluxes is maximum near to the surface and decreases with height, in stable situations the height of boundary layers is smaller compared to the convective situations. It would mean that nocturnal boundary layers are in general thinner than during the day, when the fluxes are stronger.
At this point have a clear practical consequence: over the night the pollutant diffusion from the surface (where they are emitted) to the free atmosphere is strongly suppressed, due to small turbulent fluxes. Hence, the concentrations of trace gases build up, near the surface. For modeling and forecasting the spread and concentration of pollutants, a good knowledge of the SBL structure is essential.

3.2 A rough division of SBL: weak and very stable BL

Quantitatively the measure of stability is made using stability parameters. The gradient Richardson number is a stability parameter based on the mean fields, and it is defined as the ratio of the static stability (the Brunt-Väisälä frequency N^2) and the module $|\vec{S}|$ of the shear of the mean wind:

$$Ri_g \equiv \frac{N^2}{|\vec{S}|^2} = \frac{\frac{g}{\theta_0}\frac{\partial}{\partial z}\bar{\theta}}{\left(\frac{\partial}{\partial z}\bar{u}\right)^2 + \left(\frac{\partial}{\partial z}\bar{v}\right)^2} \tag{27}$$

The quantity at denominator is a squared module, so it is always positive. The sign of Richardson number is due to the sign of static stability: in stably stratified situation potential temperature increase with height, so the gradient is positive. Then we have: $Ri > 0$ for stable conditions, $Ri < 0$ for unstable (convective) conditions.
Looking at equation (27), the gradient Richardson number takes into account not only the static stability of the atmosphere, but also the intensity of the shear. Describing the photo in figure 2, we can say that due to low wind speed (and, we can say, low wind shear), the smoke is not mixed when it reaches the equilibrium height. Then lower the wind shear is, the higher will be the stability. Reminding eq.(14), the shear of the wind acts in order to produce turbulence. Therefore Richardson number is not only a stability parameter, but *could also be* a quantity that link turbulence behaviour with local gradient of the mean quantities: positive high value of Ri could be associated with very low turbulence activity. The conjecture of the modellers is that the turbulence activity reduction could be written only as a one-value function of the gradient Richardson number.
Only with this remark we can depict a rough division of SBL (Steeneveld et al., 2006; Derbyshire, 1999a):

- weakly stable BL (wSBL): characterized by low (in respect to convective situations) but still present turbulent fluxes. In this situation the cooling of the ground increases stability, which leads a greater flux of heat from the air above. This heat flux acts in order to mix temperature, and then reduce stability. Hence, there is a negative feedback between stability and heat fluxes which could lead to a quasi-steady regime (Nieuwstadt, 1984). With quasi-steady state in the Nieuwstadt sense, we mean a state in which the vertical gradients of the mean quantities are steady in time, but the mean temperature profile continues to evolve (the ground continues to cool). WSBL are characterized by turbulent fluxes defined by their values at the surface, decreasing with height.

- very stable BL (vSBL): contrary to wSBL, in this situation an increase in stratification leads to a reduction of heat fluxes, intensifying the actual stratification. Hence, there is a positive feedback between stability and heat fluxes that could

lead to a collapse of turbulence and a decoupling of the surface (where the flow becomes laminar) with the atmosphere above. The structure of vSBL is not defined as cleary as the wSBL.

WSBL are studied in depth in literature (see i.e. Cuxart et al., 2006), even reaching some important theoretical results, like Nieuwstadt theory of weakly stratified quasi-steady SBL (Nieuwstadt, 1984).
The very stable regime is still a challenge for researchers. The decoupling of surface can lead to a production of turbulence from the upper part of the BL,due to local shear generation causing intermittent turbulence (Mahrt, 1999). The decoupling constitutes a problem even for modellers and forecast models, since it may cause a drammatic and unphysical cooling of the ground (Derbyshire, 1999b). In these situations the boundary layer structure may be modified by internal gravity waves activity. These waves can develop, grow, and even brake, helping the turbulence mixing to rise again.
As showed by Delage et al. (2002), wind intensity plays an important role in the mechanism behind the transition from a weakly stable regime to a very stable one. Small values of wind speed are necessary for a vSBL to develop.
In order to evaluate differents closure assumptions, we confine our analysis on the weakly stable regime, which is simpler to manage than the very stable.

3.3 The effect of the buoyancy term

The question that may arise is: " Why turbulent eddies should be suppressed in stably stratified situations? "
The answer lies in the Turbulent Kinetic Energy equation (14) that contains turbulence production and dissipation terms. Assuming horizontal homogeneity, and neglecting transport terms (T), eq.(14) reduce to:

$$\begin{aligned} \tfrac{d}{dt}E_k &= -\overline{u_i'w'}\tfrac{\partial}{\partial z}\bar{u}_i + \tfrac{g}{\theta_0}\overline{w'\theta'} - \epsilon \qquad i = 1,2 \\ \Rightarrow\ \tfrac{d}{dt}E_k &= -\overline{u_i'w'}\tfrac{\partial}{\partial z}\bar{u}_i \left(1 - \frac{\frac{g}{\theta_0}\overline{w'\theta'}}{\overline{u_i'w'}\frac{\partial}{\partial z}\bar{u}_i}\right) - \epsilon \\ \Rightarrow\ \tfrac{d}{dt}E_k &= -\overline{u_i'w'}\tfrac{\partial}{\partial z}\bar{u}_i \left(1 - Ri_f\right) - \epsilon \end{aligned} \tag{28}$$

The quantity $Ri_f \equiv \frac{\frac{g}{\theta_0}\overline{w'\theta'}}{\overline{u_i'w'}\frac{\partial}{\partial z}\bar{u}_i}$ is called *flux* Richardson number, and measures the fraction between buoyancy term and shear production. As have already said in section(2.1), heat

fluxes are negative in SBLs, and Ri_f is greater than zero in stable stratification. Looking at eq.(28), it suggests that for $Ri_f > 1$ shear production is unable to feed the turbulent kinetic energy, which decreases.
Thus, in stable stratification buoyancy term acts as a destruction term of TKE. As stated in sect(1.3), TKE is connected with the magnitude of turbulence activity, so a decreasing in TKE means a suppression of turbulent eddies.
In particular, a limiting value of Ri_f at which shear production, buoyancy destruction and dissipation balance each other must exist, allowing a steady turbulence. This value, called critical flux Richardson number, is a property of turbulence and does not depend on closure hypothesis: $Ri_{fcrit} \simeq 0.25$. Beyond this value, steady turbulence cannot be possible, but turbulence activity could be present in intermittent form (very stable boundary layers).

3.4 A very stable boundary layer example

The following case is a clear example of the transition from a wSBL to a vSBL. The data are measured during the night between september 14^{th} and 15^{th} 1998 at CIBA site, Spain (for details about the measurements see Cuxart et al., 2000). The stability quantity used is the "bulk" Richardson number, which is equal to the gradient Ri written using the finite-difference approximation.

Figure 3 shows the time evolution over the night between september 14^{th} and 15^{th} (from the 7.00 p.m. of 14^{th}, corresponding to 14.7 julian days, to 7.00 a.m. of 15^{th}, corresponding to 15.3 julian days) of surface temperature and bulk Richardson number measured at different altitudes. In the first part of the night (up to 9 p.m.) the values of Ri_b are smaller than 0.3, which means that a wSBL is expected to develop.
Looking at the vertical profiles in figure 4.c, 4.d, which correspond to this period of the night, we may see that fluxes and TKE have the characteristic shape, decreasing with height, with the maximum values at the surface. Wind shear is present (figure 4.a), and it feeds the turbulent quantities maintaining the SBL weakly stratified (see also potential temperature profile, figure 4.b) At 11.00 p.m., when $Ri_b \simeq 1$ the situation is completely different: turbulent fluxes values (figure 5.c, 5.d) are around zero, and the TKE slope is

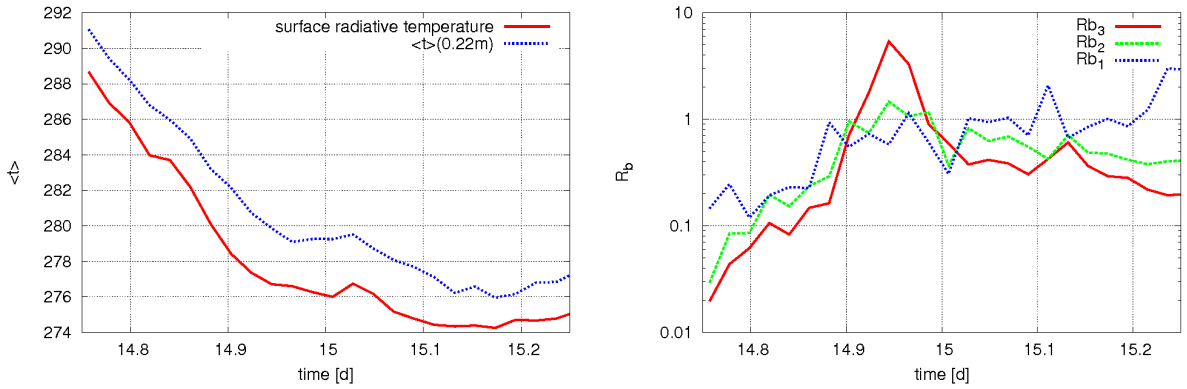

(a) (b)

Figure 3: a) Surface temperature and b)Ri_b evolutions (at different heights) over the night between september 14^{th} and 15^{th} 1998. The red "radiative" line represents an estimation of the black-body temperature of the ground. The Ri_b labels are ordered in such a way that they increase with height. The time-axis is in decimal base. Data from CIBA site, Spain.

almost vertical. The wind shear (figure 5.a) is decreased, whereas the potential temperature inversion is growing at the surface (figure 5.b). It should be noted that the second thermometer from the ground is broken. In these highly stable conditions the classical concepts of SBLs, as the Nieuwstadt (1984) theory, are not valid. Even the concept of "boundary layer height" is difficult to understand in these conditions. Finally at 3 a.m., looking only at turbulent quantities (figure 6.c, 6.d), it is not possible to state whether we are in a neutral, quasi-laminar boundary layer, or in a very SBL. It is recognizable only by looking at the strong potential temperature inversion near the surface (figure 6.b). Curiously, going back to figure 3.a, after midnight, Ri_b is quite constant with values approximately between 0.7 and 1.

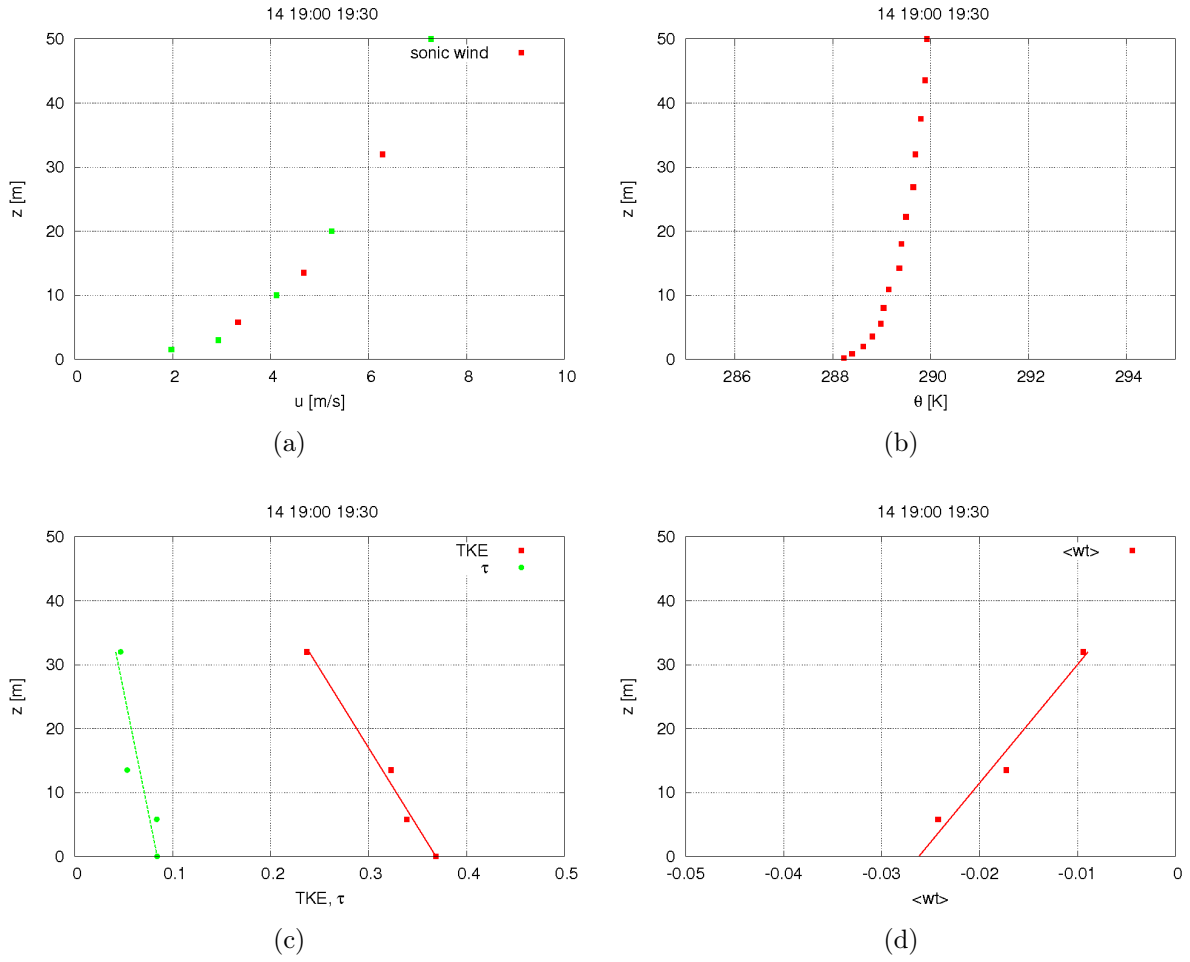

Figure 4: Vertical profiles at the beginning of the same night of figure 3 of: a) wind speed, b) potential temperature, c) module of momentum flux τ and tke, d) heat flux. All data are averaged on 30 minutes. Straight lines in c), d) are linear fit of data. Data from CIBA site, Spain.

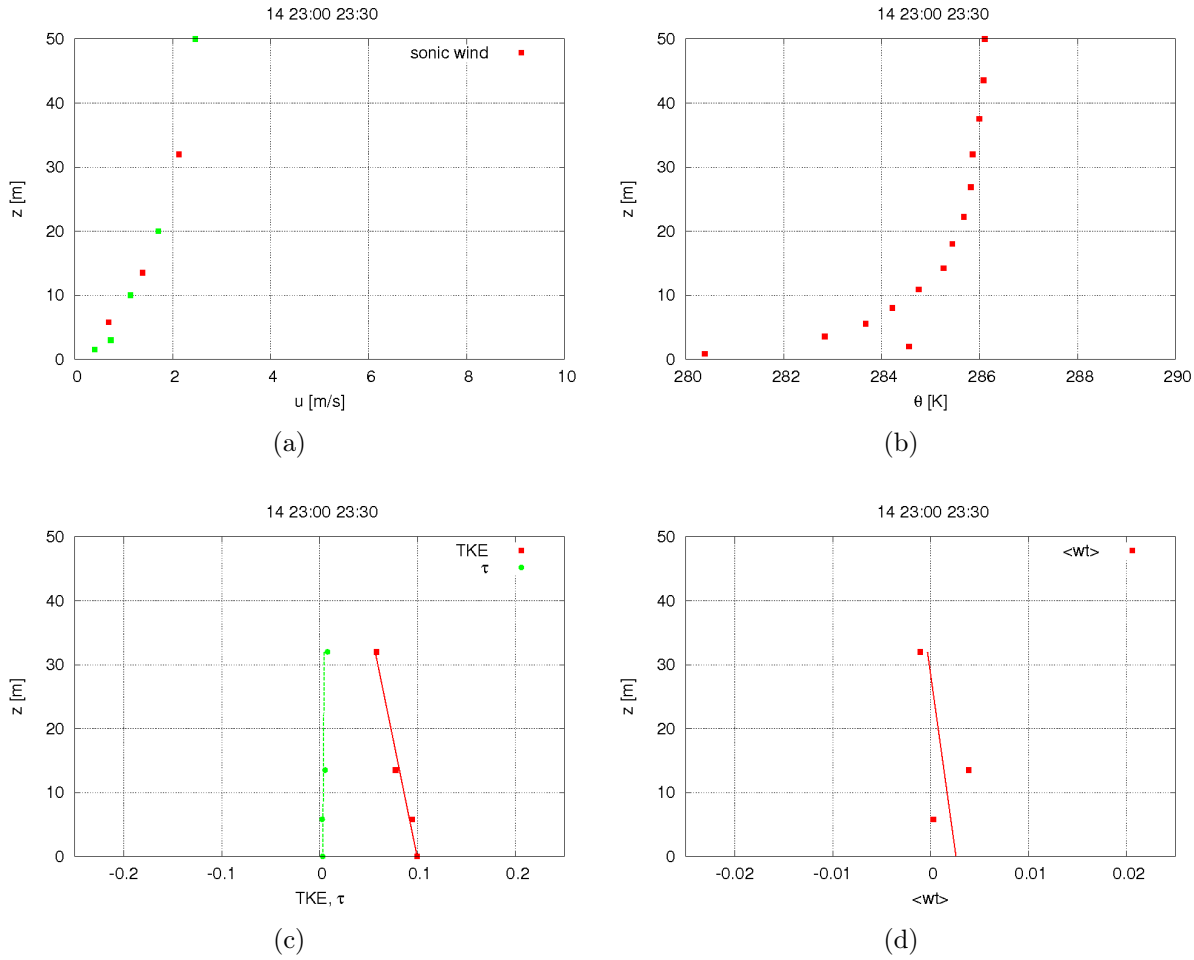

Figure 5: Vertical profiles at the middle of the same night of figure 3 of: a) wind speed, b) potential temperature, c) module of momentum flux τ and tke, d) heat flux. All data are averaged on 30 minutes. Straight lines in c), d) are linear fit of data. Data from CIBA site, Spain.

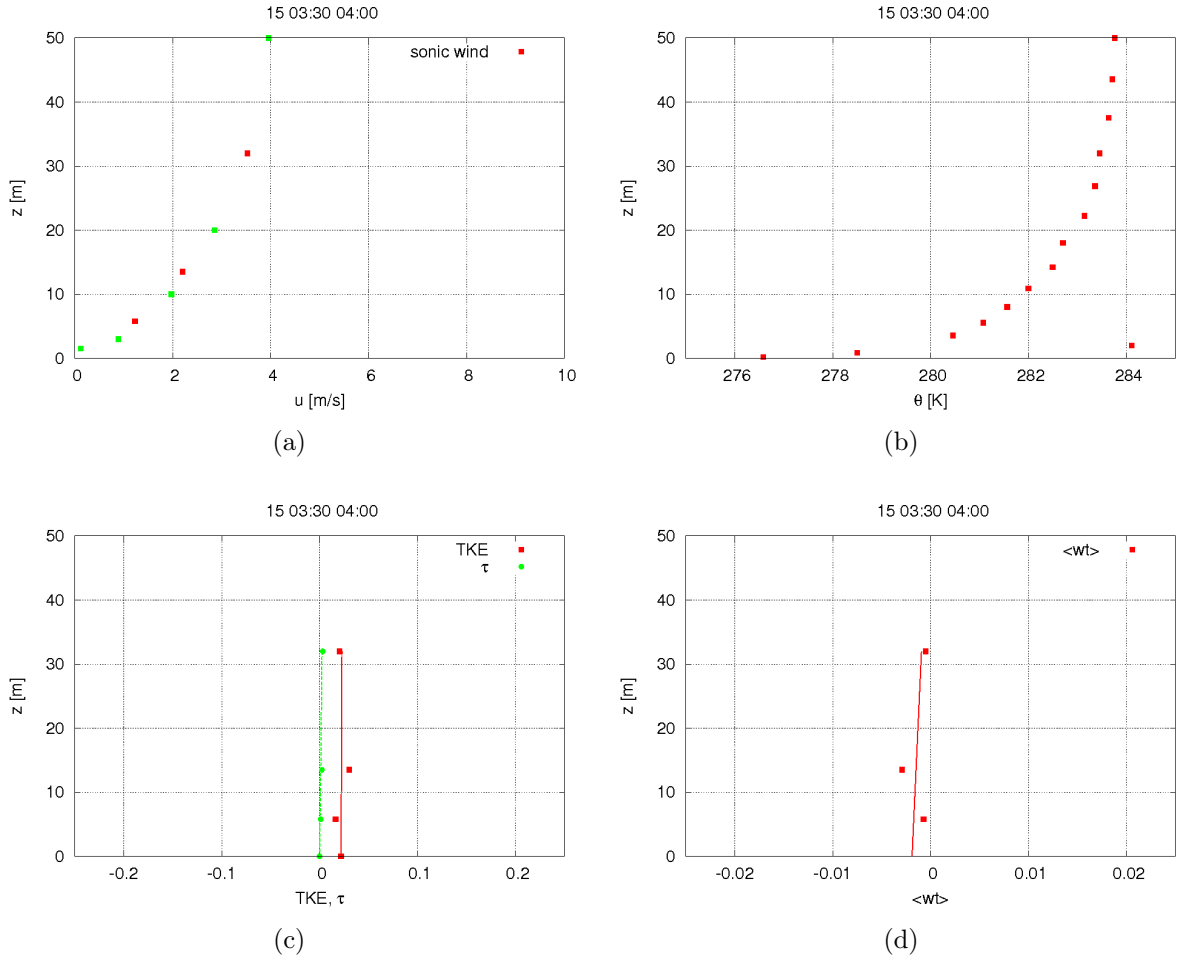

Figure 6: Vertical profiles during the same night of figure 3 of: a) wind speed, b) potential temperature, c) module of momentum flux τ and tke, d) heat flux. All data are averaged on 30 minutes. Straight lines in c), d) are linear fit of data. Data from CIBA site, Spain.

4 Models

4.1 The paradigm

Reminding the equations governing a one-dimensional model of the atmosphere (24), (25), (26), the problem is "reduced" to find a parametrization (remember section (1.3)) for the turbulent fluxes $\overline{u_i' w'}$, $\overline{\theta' w'}$.
In analogy with the molecular viscosity of equation (7), we can think turbulent flux term like a "diffusion" of momentum and heat, characterized with particular coefficients of *eddy viscosity* and *eddy diffusivity* (Monin and Yaglom, 1971):

$$\overline{u'w'} = -K_m \frac{\partial \overline{u}}{\partial z} \qquad \overline{\theta' w'} = -K_h \frac{\partial \overline{\theta}}{\partial z} \tag{29}$$

There is a critical point in this kind of formulation: unlike the coefficient ν of molecular viscosity, the eddy viscosity $K_{m,h}$ does not characterize any physical properties of the fluid, such that it cannot be considered a property of the fluid. It depends on the charateristics of the flow, and may vary (in principle) in space and time. Hence, taking into account such *flux-gradient relation* as a paradigm of turbulence modelling [1], the goal is to find a rightful parametrization for the turbulent diffusion coefficient $K_{m,h}$. The idea is to use the same argument of molecular viscosity which is defined by kinetic theory of gas (Pope, 2000):

$$\nu \simeq \frac{1}{2} \bar{c} \lambda \tag{30}$$

where $\bar{c}$ is the mean molecular speed, and λ is the mean free path. Thinking about Reynolds stresses as a turbulent diffusion process, it seems reasonable to use the same argument of eq.(30) for turbulent viscosity/diffusivity K_m, K_h. Therefore, the problem is shifted to find a rightful choice of a velocity scale U analogous to $\bar{c}$ and length scale L analogous to the mean free path.

$$K_m \sim K_h \sim U\, L \tag{31}$$

[1] The eddy-diffusion assumption is deeply based on two hypothesis: in first place that the Reynolds stresses are totally defined by local mean values, and secondly that there is a linear relation between the non-diagonal terms of Reynolds tensor and strain tensor (the flow is a Newtonian fluid). These two hypothesis are not physically grounded when turbulence time-scale is large compared to a characteristic mean flow time-scale, i.e. shear time-scale (see **?**).

Whilst the velocity scale U may be linked to some turbulent quantities (as the square root of momentum fluxes at the surface), the length scale L called *mixing length* is not easy to define: it should be thought as the characteristic distance covered by a fluid parcel transported by a turbulent eddy. Such distance does not only depend on the geometry of the flows, but as we see in chapter(3) it even depends on the stability of the flow.
In example in the neutral surface layer, that is the costant flux region of boundary layer (corresponding to $\sim 10\%$ of it), K_m, K_h are computed (Monin and Yaglom, 1971):

$$K_m \sim K_h \sim u_* \, kz \tag{32}$$

where u_* is the squared root of the module of momentum fluxes at the surface $u_* \equiv (\overline{u'w'}^2 + \overline{v'w'}^2)^{1/4}$, and kz is the mixing length near the ground: without stability effects, the eddies are bounded only by the presence of the ground at the bottom and their size is proportional to the geometric height z. Hence in surface layer we find that the ratio between K_m and K_h, called the *Prandtl turbulent* number is costant:

$$Pr_t^{sfc} \equiv \frac{K_m^{sfc}}{K_h^{sfc}} \sim constant \tag{33}$$

4.2 The effect of stratification

The previous argument is exact only for a neutral boundary layer. If we consider the effect of stratification the paradigm that we follow is based on the *similarity theories*: Monin-Obukhov similarity for the surface layer (Monin and Obukhov, 1954), and his extensions to the entire boundary layer due to Nieuwstadt (Nieuwstadt, 1984).
Shortly, a similarity theory is a scale analysis based on the organization of variables into dimensionless groups. This organization is guided by "Buckingum π theory" (see i.e. Stull, 1988): applied on the boundary layer equations it says that all turbulent quantities, adimensionalized using characteristic scale quantities (and with "characteristic" we mean the quantities *relevant* to the problem), may be expressed as a functions of a single dimensionless parameter that fully characterize stratification:
I.e. if X is the turbulent quantity and A, B, C are the scale quantities on which X depend, we may find a dimensionless quantity ζ resulting from a combination of A, B, C

such that:

$$\frac{X}{A^a B^b C^c} = \psi_X(\zeta) \tag{34}$$

It should be stressed that a similarity theory does not give an analytical shape for the functions ψ. It just states that such functions *exist*. Moreover, the choice of the relevant quantities is based only on physical arguments, and it is not always clear.
Applied (34) on (31) we obtain:

$$K_{m,h} = UL\, f_{m,h}(\zeta) \tag{35}$$

Basic point is that the functional dependence from ζ is different for heat and momentum coefficient. If ζ is some measure of stability, it follows that the turbulent Prandtl number Pr_t, which is costant in neutral surface layer (eq.(33)), is a function of ζ as well:

$$Pr_t \equiv \frac{K_m}{K_h} = Pr_t(\zeta) \tag{36}$$

Then, the mixing of momentum or heat varies in different manner with the parameter ζ.

4.2.1 Monin-Obukhov scaling

The first boundary layer similarity theory was developed by Monin and Obukhov (1954) for a stationary atmospheric surface layer over horizontally homogeneus terrain. In these conditions the structure of turbulence is completely characterized by the surface turbulent stresses u_*^2, the surface heat flux $\overline{\theta' w'}|_{sfc}$, the buoyancy term g/θ_0 and the height above the ground z. These quantities are necessary to define a velocity scale u_*, a temperature scale $\theta_* \equiv \overline{\theta' w'}|_{sfc}/u_*$, and a length scale of turbulence, the *Monin-Obukhov* length L_{MO}:

$$L_{MO} \equiv -\frac{u_*^2}{k\frac{g}{\theta_0}\theta_*} \tag{37}$$

Applying (34) all statistics quantities properly scaled, as mean values, gradients, variances, they may be written as universal functions of a non-dimensional parameter which

is the ratio between geometric height z and L_{MO}:

$$\zeta \equiv \frac{z}{L_{MO}} \tag{38}$$

Shortly, MO similarity says that turbulence within the surface layer is fully characterized by the surface turbulent stress $\overline{u'w'}|_{sfc} \equiv u_*^2$ and the surface heat flux $\overline{\theta'w'}|_{sfc} \equiv u_*\theta_*$. Hence, the MO-length L_{MO} represents the distance from the surface at which the buoyant production of turbulence (of TKE) equals the shear production: it is the height at which buoyancy dominates in respect with the shear .
Hence, ζ is a stability parameter, like the gradient Richardson number defined in eq.(27). Unlike Ri, ζ is defined with *internal* quantities of turbulence, the fluxes, while Ri is defined with mean flow quantities. For $\zeta > 0$ the BL is *stably* stratified. Instead, if $\zeta < 0$, the BL is *unstably* (convectively) stratified.

4.2.2 Nieuwstadt local scaling

Nieuwstadt (1984) extended MO-similarity, strictly valid only in the surface layer to the whole boundary layer: starting from the diagnostic equations for the second order moments, he derived (see for details Nieuwstadt, 1984) that all turbulent quantities may be expressed in terms of the *local* fluxes $\overline{u'w'}(z)\,, \overline{\theta'w'}(z)$. Hence, he defined a new stability parameter called *local MO-length scale* Λ such that:

$$\Lambda \equiv -\frac{\tau(z)^{3/2}}{k\frac{g}{\theta_0}\overline{\theta'w'}(z)} \Rightarrow \zeta|_{loc} = \frac{z}{\Lambda} \quad , \quad \tau = \sqrt{\overline{u'w'}^2 + \overline{v'w'}^2} \tag{39}$$

Nieuwstadt theory gives a "similarity" interpretation to the flux gradient relation (29). It is important to observe that local scaling hypothesis is closely related to the assumption that turbulence is in local equilibrium, because it is derived from the assumption that all second order moments are locally in a steady state. In particular for TKE equation, it means that production and dissipation should be in local balance. If they are not in local balance (i.e. through a big influence of pressure-velocity correlation term), the local scaling hypothesis will hardly be reasonable (Derbyshire, 1999a).

What is usually done in turbulence modelling is to write local quantities in terms of

gradient Richardson number instead of Λ: local scaling permits to write Ri as a function of Λ, therefore it is possible to write non-dimensional turbulent quantities in terms of Ri (see i.e. Sorbjan, 2010).

Applying these arguments to the turbulent diffusion coefficients $K_{m,h}$ yelds:

$$K_{m,h} = U\, L\psi_{m,h}(Ri) \tag{40}$$

This formulation for $K_{m,h}$ allows to overcome the problem of a critical Richardson number Ri_c. Recalling the definition of flux Richardson number (28), we obtain Richardson number just using flux-gradient relations:

$$Ri_f \equiv \frac{\frac{g}{\theta_0}\overline{w'\theta'}}{\overline{u'w'}\frac{\partial\overline{u}}{\partial z}} = \frac{\frac{g}{\theta_0}K_h\frac{\partial\overline{\theta}}{\partial z}}{K_m\frac{\partial\overline{u}}{\partial z}^2} = \frac{K_h}{K_m}Ri \Rightarrow Ri = \frac{K_m}{K_h}Ri_f \tag{41}$$

In a "classical" formulation (i.e. in Nieuwstadt (1984)), $K_m/K_h \sim 1$ (or equivalenty Pr_t is costant, the so-called Reynolds analogy) so if Ri_f reaches its critical value, so does the gradient Richardson number: $Ri_{fcrit} \simeq Ri_{gcrit} \simeq 0.25$.
If $K_m/K_h \sim \psi(Ri)$, our previus reasoning is not strictly valid. In particular, if $K_m > K_h$ in stable conditions (if we assume that momentum is mixed more than heat with stable stratification (Kondo et al., 1978)) we may overcome the existence of such critical Richardson number. This is what is done in ordinary turbulence closure schemes.

4.3 Second order schemes

There are many different closure schemes in literature. In the present work we deal with the so-called "higher-orders" closure schemes, in which prognostic equations for turbulent quantities (higher order moment) are used, coupled with the equations for the first moments (see Mellor and Yamada, 1982, for an exhaustive treatment of the hierarchy of turbulence modelling).
In a second order closure model $TKE - l$ [2] the idea below is that turbulent kinetic energy is the quantity that fully characterizes all other turbulence quantities (reminding,

[2] in literature they are even called "I-1/2" order schemes, a full "II-order" scheme use prognostic equations even for turbulent fluxes, eq (13),(15)

for instance of the comments on TKE-equation in chapter(2)): hence, it is straighforward to identify the velocity scale U of turbulent diffusion with the square root of turbulent kinetic energy. The length scale L is still an ambiguos term: we need to link the near-surface behaviour with the length scale of eddies far from the surface, and the effect of stability on such mixing length. Following Blackadar (1962) we define a mixing length which is the interpolation between these three different contributions.
Using TKE-budget equation it is possible to determine explicitly turbulent kinetic energy, parametrizing the higher-than-II-order turbulent terms that appear in the budget equation.
We analize in details the $TKE - l$ scheme used by Bologna Limited Area Model (BOLAM) taking it as representative of this class of closure schemes.

4.4 TKE-l BOLAM closure

Recalling the TKE-budget equation (14), and applying the SCM simplifications we have:

$$\frac{\partial E_K}{\partial t} + (T)_{vert} = -\overline{u_i' w'}\frac{\partial \overline{u_i}}{\partial z} + \frac{g}{\theta_0}\frac{\overline{\theta' w'}}{\partial z} - \epsilon \qquad i = 1, 2 \tag{42}$$

Coupled with eq (24),(25),(26).
Hence, in order to close the system of equations, we need a parametrization for the third order moment $(T)_{vert}$ (vertical "flux of kinetic energy" and correlation between pressure fluctations and vertical velocity fluctuations), and the dissipation rate ϵ.

In the BOLAM's scheme, the velocity scale of turbulent diffusion coefficient $K_{m,h}$ is linked to the *local friction velocity* u_* (which is a generalization based on local scaling of the surface friction velocity). Surface layer measurements have determined that friction velocity could be written as a fraction c_e of the turbulent kinetic energy E_K. Hence the eddy viscosity coefficient K_m:

$$u_*^2 = c_e E_K \rightarrow K_m = l\sqrt{c_e E_K}, \qquad c_e = 0.17 \tag{43}$$

On the contrary the eddy diffusivity K_h is written using *Prandtl turbulent number* Pr_t.

Basing on local scaling approach, we could write Pr_t as a function of Richardson number, $Pr_t = Pr_t(Ri)$:

$$K_h = \frac{K_m}{Pr_t} \tag{44}$$

where Pr_t is a Richardson number's function such that:

$$Pr_t = 1 + 5\,Ri \tag{45}$$

for the stable case. This relation implies less turbulent heat mixing than momentum mixing in stably stratified conditions (Pr_t is monotonic positive defined function of Ri). For the mixing length in stable cases, BOLAM uses the Blackadar (1962) parametrization, modified by a stability function:

$$l_{black}^{-1} = \frac{1}{kz} + \frac{1}{l_{max}} \;\Rightarrow\; l_{bolam} = \frac{kz\,l_{max}}{kz + l_{max}} \frac{1}{1 + 12Ri} \quad l_{max} = 100m \tag{46}$$

For the unstable cases, it uses a *non-local* parametrization, non-dipendent on stratification:

$$l_{conv} = C_u \left[(z_{up} - z)(z - z_{down})^3\right]^{1/4} \qquad z_{down} < z < z_{up} \quad C_u = 0.5 \tag{47}$$

where z_{down},z_{up} represent the bottom and top heights of the convective layer.
It should be pointed that this mixing length formulation is not a continue function of the stratification:
Such choice, from weather forecast's point of view, with very low vertical resolution, may be useful. From a researcher's point of view, eq.(46), (47) lack in "physics", and it may even be considered "wrong" if we thought (as we do) of mixing length as a continue function of stability.
As we have already written, we need a parametrization for triple moments and the rate of dissipation. The triple moment of equation (42) describes the vertical flux of kinetic energy: in analogy with what has been done with the fluxes of momentum and heat, we shall write it using a flux-gradient relation:

$$(T) \equiv \frac{\partial}{\partial z}\left(\frac{1}{2}\overline{u_i' u_i' w'} + \frac{1}{\rho_0}\overline{p' w'}\right) = -\frac{\partial}{\partial z}\left(K_e \frac{\partial E_k}{\partial z}\right) \tag{48}$$

The rate of dissipation ϵ instead, is written with Kolmogorov's inertial sub-range theory

Kolmogorov (1941):

$$\epsilon = c_\epsilon \frac{E_K^{3/2}}{l} \qquad c_\epsilon = (c_e)^{3/2} = 0.07 \tag{49}$$

The turbulent diffusion coefficient K_e is parametrized maintaining the analogy with the momentum coefficient:

$$K_e = l\sqrt{c_e\, E_k} \qquad c_e = 0.17 \tag{50}$$

Using the closures described, the sistem of prognostic equations which must be resolved is:

$$\begin{aligned} \frac{\partial \overline{u}}{\partial z} &= +f(\overline{v} - v_g) + \frac{\partial}{\partial z}\left(K_m \frac{\partial \overline{u}}{\partial z}\right) \\ \frac{\partial \overline{v}}{\partial z} &= -f(\overline{u} - u_g) + \frac{\partial}{\partial z}\left(K_m \frac{\partial \overline{v}}{\partial z}\right) \\ \frac{\partial \overline{\theta}}{\partial t} &= +\frac{\partial}{\partial z}\left(K_h \frac{\partial \overline{\theta}}{\partial z}\right) \end{aligned} \tag{51}$$

$$\frac{\partial E_K}{\partial t} - \frac{\partial}{\partial z} K_e \frac{\partial E_K}{\partial z} = +K_m (\frac{\partial \bar{u}}{\partial z})^2 + K_m (\frac{\partial \bar{v}}{\partial z})^2 - K_h \frac{g}{\theta_0} \frac{\partial \overline{\theta}}{\partial z} - \frac{c_\epsilon E_K^{3/2}}{l}$$

With turbulent fluxes and mixing length diagnosed using:

$$\begin{aligned} \overline{u_i' w'} &= -K_m \frac{\partial \overline{u_i}}{\partial z} \qquad K_m = l\sqrt{c_e E_K} \\ \overline{\theta' w'} &= -K_h \frac{\partial \overline{\theta}}{\partial z} \qquad K_h = K_m / Pr_t \\ l &= \frac{kz\, l_{max}}{kz + l_{max}} \frac{1}{1 + 12Ri} \quad l_{max} = 100m \end{aligned} \tag{52}$$

4.5 Total Turbulent Energy as characteristic turbulence quantity

A II order $TTE - l$ closure (Mauritsen and Svensson (2007a), Zilitinkevich et al. (2007), Zilitinkevich et al. (2013)) is based on the hypothesis according to which the quantity characterizing turbulence is the total turbulent energy (TTE), instead of TKE alone. Using the concept of TTE, there is no "destruction" of buoyancy due to the stratification, but only a conversion of TKE in TPE, like the usual classic mechanics concepts of

conservation of total energy. Applying to eq.(21),(22) the SCM simplification yelds:

$$\frac{\partial E}{\partial t} = -\left(\overline{u'w'}\frac{\partial \overline{u}}{\partial z} + \overline{v'w'}\frac{\partial \overline{v}}{\partial z}\right) - (T) + \left\{ \begin{array}{cc} 0 & if\ \frac{\partial \theta}{\partial z} \geq 0 \\ 2\frac{g}{\theta_0}\overline{w'\theta'} & if\ \frac{\partial \theta}{\partial z} < 0 \end{array} \right\} - \epsilon_E \tag{53}$$

Coupled as above with eq.(24),(25),(26).
Even though it only uses one prognostic equation like a "classical" TKE-l scheme, the reason why TTE is employed instead of TKE is that TTE is a conserved property (it becomes an invariant in absence of production and dissipation), in contrast with TKE that continuosly feeds the potential energy TPE.

4.5.1 Energy scaling

At present time, the sole model using a TTE-l scheme for stable cases is the one developed by Mauritsen and Svensson (2007a). Together with TTE-budget equation, they have developed a new closure for fluxes based on a *local energy* similarity theory. Basing themselves on experimental evidences, Mauritsen and Svensson (2007b) assumed that non dimensional turbulent momentum and heat fluxes are unique functions of Richardson number:

$$\frac{|\vec{\tau}|}{E_K} = \frac{\sqrt{\overline{u'w'}^2 + \overline{v'w'}^2}}{E_K} = f_\tau(Ri) \qquad \frac{\overline{w'\theta'}}{\sqrt{E_K \overline{\theta'^2}}} = f_\theta(Ri) \tag{54}$$

Where the functions $f_\tau(Ri)\,, f_\theta(Ri)$ are for the stable case:

$$f_\tau(Ri) = 0.17(0.25 + 0.75(1+4Ri)^{-1})\,, \qquad f_\theta(Ri) = -0.145(1+4Ri)^{-1} \tag{55}$$

And for the the convective case:

$$f_\tau = 0.17 \qquad f_\theta = +0.145 \tag{56}$$

Our analysis in figure 7, based on data from CIBA site in Spain, confirms the Ri-dependence of the non-dimensional turbulent fluxes.
Moreover, figures 7.a, 7c, 7e show that the drop of the non-dimensional momentum fluxes, as Ri increases, is quicker than Mauritsen's functions.
Physically, it means that in the surface layer, if we compute (or measure) only friction velocity, the corresponding value of turbulent kinetic energy available to the system is

higher than in the non nearly-neutral case.
In all the plots we have added the BOLAM formulation for the same quantities. As we can easily see, BOLAM uses a costant value for the ratio $\frac{|\vec{\tau}|}{E_K}$, which corresponds to the value $c_e = 0.17$. This value corresponds to nearly neutral stratification, where the turbulence is isotropic. Figure 7 says that in stable stratification turbulence is highly anisotropic, and such anisotropy modifies the partition of turbulent kinetic energy on the non-diagonal terms of the Reynolds stress tensor.
For stable cases, at $Ri << 1$, Mauritsen f_θ function tends to a costant value: $f_\theta(0) = -0.145$. From f_θ definition, it implies that turbulent flux and variance of temperature tend to zero with the same velocity. Looking at 7.b, 7.d, 7.f, it is not possible to corroborate this hypothesis because of the different behaviours of $\frac{\overline{w'\theta'}}{\sqrt{E_K \overline{\theta'^2}}}$ at the different altitude for small values of Ri.
It should be pointed that this quantity is not very familiar at near neutral regime, in particular if you would compare the analytical function with experimental data. Whilst $\frac{|\vec{\tau}|}{E_K}$ tends to the neutral limit value $c_e = 0.17$, for $Ri \to 0$ both heat flux and temperature variance go to zero.
From an experimental point of view, data of $\frac{\overline{w'\theta'}}{\sqrt{E_K \overline{\theta'^2}}}$ for $Ri \to 0$ have no sense. So any validation of numerical costants (as the limit value $f_\theta(0) = -0.145$) using data in the limit of Richardson number tending to zero, have no sense.

Analysis of the pdf of the quantity $\frac{|\vec{\tau}|}{E_K}$ permits to say more on the TKE partition on non-diagonal terms: in figure 8 the probability density functions (pdfs) are showed (with the corresponding cumulative functions) computed for different ranges of Richardson number values at different altitudes,for a dataset of measuraments from Cabauw tower (Netherlands).
For low stabilities, (8.a: $0.1 < Ri < 0.16$; 8.b: $0.25 < Ri < 0.4$) the pdfs show clear peaks which correspond to the most probable values (the modal value) and approximately to median values of the cumulative functions. Physically, we may understand it saying that the existence of a modal value validate the idea that this quantity may be written as a function of the Richardson number.
On the other hand, looking at plots at higher stability range, (8.c: $0.6 < Ri < 1$, 8.d: $1 < Ri < 1.6$) the situation is completely different: there are not clear peaks of the pdfs which are almost flat. Phisycally it would mean that there is no reason to think that

the quantity $\frac{|\vec{\tau}|}{E_K}$ may be a function of Richardson number, at high values of it. Looking at a functional depedences at high stabilities between these quantities, after figure 8, it seems unjustified.

4.5.2 TTE-l Mauritsen's closure

Together with usual triple moments and dissipation rate parametrization, also a parametrization for kinetic and potential energy partition are necessary, in order to calculate turbulent fluxes using eqs(55).
In equation (53) the shear production term is parametrized with the assumption (that it is implicit in the linear relation between stresses and strain rate) that the stress vector is aligned with the gradient velocity vector. So, if two vectors are aligned, their scalar product is equal at their modules product:

$$\left(\overline{u'w'}\frac{\partial \overline{u}}{\partial z} + \overline{v'w'}\frac{\partial \overline{v}}{\partial z}\right) = \vec{\tau}\cdot\vec{S} = |\vec{\tau}|\,|\vec{S}| \tag{57}$$

The dissipation rate ϵ as usual is parametrized with Kolmogorov's theory:

$$\epsilon = C_\epsilon \frac{E^{3/2}}{l} \qquad C_\epsilon = f_\tau(0)^{3/2} = 0.07 \tag{58}$$

It should be pointed that this equation implies the same dissipation time scale for potential and kinetic energy. As already showed by Zilitinkevich et al. (2013), this assumption is not strictly valid.
The turbulent flux of the total energy is closed with a flux-gradient relation:

$$(T) = \frac{\partial}{\partial z}\left(-K_E\frac{\partial E}{\partial z}\right) \qquad K_E \equiv |\vec{S}|\,l^2 \Rightarrow \frac{\partial \phi_E}{\partial z} = \frac{\partial}{\partial z}\left[-K_E\frac{\partial E}{\partial z}\right] \tag{59}$$

The mixing length l is inspired to Blackadar formulation, taking an interpolation between geometric distance height z, Coriolis effect f, and static stability N for the stable case:

$$\frac{1}{l} = \frac{1}{kz} + \frac{f}{C_f\tau^{1/2}} + \frac{N}{C_N\tau^{1/2}} \tag{60}$$

We have not treated the unstable case, so we have just chosen a function which should

be continued for all the range of stability:

$$\frac{1}{l} = \frac{1}{kz} + \frac{f}{C_f \tau^{1/2}} \tag{61}$$

On the contrary, if we consider the bulk of the boundary layer (like the BOLAM mixing length in example), this formulation is based on the local values of the momentum fluxes and the temperature gradient, at the considered height z. Hence, it allows decoupled turbulence in, for example, low level jet. $C_f = 0.185$, $C_N = 1.3$ are determined by Mauritsen and Svensson (2007a) by tuning with many LES results.

Total energy partition in kinetic and potential energy is calculated using a function f_{int}, interpolating between the two asymptotic values $Ri \ll 1$, $Ri \gg 1$. These limiting values are obtained using TKE and TPE budget equations in steady conditions, omitting third order moment (assumed to be negligible in steady conditions). As usual, we shall consider the two different situations, Ri less or greater than zero. For $Ri > 0$ we have:

$$\frac{E_P}{E_K} = \frac{\frac{g}{\theta_0}\overline{w'\theta'}}{|\vec{\tau}||\vec{S}| + \frac{g}{\theta_0}\overline{w'\theta'}} \Rightarrow Ri_f \equiv -\frac{\frac{g}{\theta_0}\overline{w'\theta'}}{|\vec{\tau}||\vec{S}|} = \frac{Ri}{Pr_T} \Rightarrow \frac{E_P}{E_K} = \frac{Ri_f}{1 - Ri_f} \tag{62}$$

$$\Rightarrow \frac{E_P}{E_K} = \begin{cases} Ri << 1 : \frac{Ri}{Pr_T(1-\frac{Ri}{Pr_T})} \rightarrow \frac{Ri}{Pr_T(0)} \\ Ri >> 1 : Ri_f \rightarrow Ri_{fcrit} \Rightarrow \frac{Ri_{fcrit}}{1-Ri_{fcrit}} \simeq 0.46 \end{cases}$$

$$\Rightarrow \left(\frac{E_P}{E_K}\right)^{-1} = f_{int}(Ri) \qquad \Rightarrow \quad E_P = E_K f_{int}^{-1}(Ri)$$

f_{int} is an unique function of Richardson number, critical flux Richardson number, and Pr_t in the neutral limit:

$$f_{int} \equiv \left(\frac{1}{\frac{Ri}{Pr_T(0)}} + \frac{1}{\frac{Ri_{fcrit}}{1-Ri_{fcrit}}} \right) \tag{63}$$

As far as the convective case is concerned, the procedure is analogous: an interpolation is done between the limiting values $Ri \rightarrow 0^-$ e $Ri \rightarrow -\infty$. Now, in the asymptotic limit

we assume that shear production is negligible with respect to heat flux:

$$\frac{E_P}{E_K} = \begin{cases} |Ri| << 1 : \frac{|Ri|}{Pr_T(1-\frac{|Ri|}{Pr_T})} \rightarrow \frac{|Ri|}{Pr_T(0)} \\ \\ |Ri| >> 1 : \frac{\frac{g}{\theta_0}\overline{w'\theta'}}{\frac{g}{\theta_0}\overline{w'\theta'}(|\tau||S|/\frac{g}{\theta_0}\overline{w'\theta'}+1)} \rightarrow 1 \end{cases} \tag{64}$$

So, for convective cases the ratio of potential to kinetic energy is written as:

$$E_P = g_{int}^{-1} E_K \qquad g_{int} \equiv \left(\frac{1}{\frac{|Ri|}{Pr_t(0)}} + 1 \right) \tag{65}$$

From eq.(62) and the condition $E = E_K + E_P$ obtaining E_K and E_P is straightforward:

$$E_K = E\frac{1}{1 + f_{int}^{-1}(Ri)} \qquad E_P = E\frac{f_{int}^{-1}(Ri)}{1 + f_{int}^{-1}(Ri)} \tag{66}$$

Using eq.(19), we may obtain variance of temperature fluctations (the *energy* of temperature fluctations), used in the calculus of heat fluxes:

$$\overline{\theta'^2} = 2\left(\frac{\frac{g}{\theta_0}|\frac{\partial\theta}{\partial z}|}{(\frac{g}{\theta_0})^2} \right) E_P = 2\left(\frac{g|\frac{\partial ln\theta}{\partial z}|}{\frac{g}{\theta_0}^2} \right) E_P$$

(67)

With (59),(58),(62),(67) the set of equations (24), (25), (26), (53) is closed.

However, since our numerical code is written in terms of flux-gradient relations, we need a formulations for turbulent diffusion coefficients K_m , K_h. Eddy viscosity K_m may be calculated inverting eq.(31):

$$K_m = +\frac{|\vec{\tau}|}{|\vec{S}|} \tag{68}$$

We cannot do the same operation with eddy diffusion K_h, because when heat fluxes go to zero (i.e. in near neutral stratification), K_h does not tend to zero, it tends to a value near K_m ($Pr_t(0) \sim 1$). Hence, we compute it following Mauritsen and Svensson (2007a), just multiplying TPE equation in steady conditions, neglecting third order terms, by K_h

on the lhs and rhs of the equation:

$$K_h = \frac{\overline{w'\theta'}^2}{\epsilon_P} = \frac{2 f_\theta^2 E_K l}{C_\epsilon \sqrt{E}} \tag{69}$$

using eq.(68),(69) we may express the stress and heat flux gradients as a diffusion of momentum and heat in the vertical coordinate.

$$\overline{u_i' w'} = -K_m \frac{\partial \overline{u_i}}{\partial z} \qquad \overline{\theta' w'} = -K_h \frac{\partial \overline{\theta}}{\partial z} \tag{70}$$

The complete set of equation to be solved becomes:

$$\begin{aligned} \frac{\partial \overline{u}}{\partial t} &= +f(\overline{v} - \overline{v_g}) + \frac{\partial}{\partial z} K_m \frac{\partial \overline{u}}{\partial z} \\ \frac{\partial \overline{v}}{\partial t} &= -f(\overline{u} - \overline{u_g}) + \frac{\partial}{\partial z} K_m \frac{\partial \overline{v}}{\partial z} \\ \frac{\partial \overline{\theta}}{\partial t} &= +\frac{\partial}{\partial z} K_h \frac{\partial \overline{\theta}}{\partial z} \end{aligned} \tag{71}$$

$$\frac{\partial E}{\partial t} = + \left(f_\tau E_K |\vec{S}| \right) + \frac{\partial}{\partial z} K_E \frac{\partial E}{\partial z} + \left\{ \begin{array}{cc} 0 & \frac{\partial \theta}{\partial z} \geq 0 \\ 2 \frac{g}{\theta_0} f_\theta \sqrt{E_K \overline{\theta'^2}} & \frac{\partial \theta}{\partial z} < 0 \end{array} \right\} - C_\epsilon \frac{E^{3/2}}{l}$$

$$E = E_K + E_P \Rightarrow E_K = E - E_P \qquad E_P = \left\{ \begin{array}{l} E_K f_{int}^{-1}(Ri) \\ \\ E_K g_{int}^{-1}(Ri) \end{array} \right.$$

It should be pointed that at opposite with TKE equation in (51), the shear production term has positive sign, instead of minus as usual adopted.

4.6 Surface layer parametrization

Monin-Obukhov similarity is used to compute turbulent fluxes at the boundary (defined as fluxes at first computational level from soil), using an arbitrary set of similarity functions ϕ:

$$\frac{kz}{u_*} \frac{\partial \overline{u}}{\partial z} = \phi_m \left(\frac{z}{L} \right) \tag{72}$$

$$\frac{kz}{\theta_*}\frac{\partial\overline{\theta}}{\partial z} = -\phi_h\left(\frac{z}{L}\right)$$

Our schemes use for the $\phi - functions$ in the stable case, Holtslag's functions (Beljaars and Holtslag, 1991) (with $\frac{z}{L} \equiv \zeta$):

$$\int_{\zeta_0}^{\zeta}\frac{\phi_m(\zeta')-1}{\zeta'}d\zeta' \equiv \psi_m(\zeta,\zeta_0) = -\left[a\left(\frac{z}{L}-\frac{z_0}{L}\right)+b\left(\frac{z}{L}-\frac{c}{d}\right)e^{(-d\frac{z}{L})}-b\left(\frac{z_0}{L}-\frac{c}{d}\right)e^{-d\frac{z_0}{L}}\right] \tag{73}$$

$$\int_{\zeta_0}^{\zeta}\frac{\phi_h(\zeta')-1}{\zeta'}d\zeta' \equiv \psi_h(\zeta) = -\left[(1+a\frac{2}{3}\frac{z}{L})^{3/2}+b(\frac{z}{L}-\frac{c}{d})e^{(-d\frac{z}{L})}\right]+$$
$$+\left[(1+a\frac{2}{3}\frac{z_0}{L})^{3/2}+b(\frac{z_0}{L}-\frac{c}{d})e^{(-d\frac{z_0}{L})}\right]$$

with the coefficients: $a = 1$, $b = 2/3$, $c = 5$, $d = 0.35$.

Classical MO surface formulations use for the stable case linear ϕ functions of ζ. These formulations in the limit of very high stability lead to the so-called "z-less" limit (Wyngaard, 1975): for $\zeta >> 1$ the counteraction of stratification is too strong, causing a detachement of the turbulence characteristics of the above atmosphere from the surface. Therefore the reason of the name "z-less": the turbulence becomes indipendent from the height.

This is not validated by the observations, since linear ϕ function formulation overestimates the suppression of turbulent mixing, causing a too quick detachment from the surface and hence an overcooling of the surface (Derbyshire, 1999b). Hence it is preferred to use Holtslag's functions, which are more coherents with data.

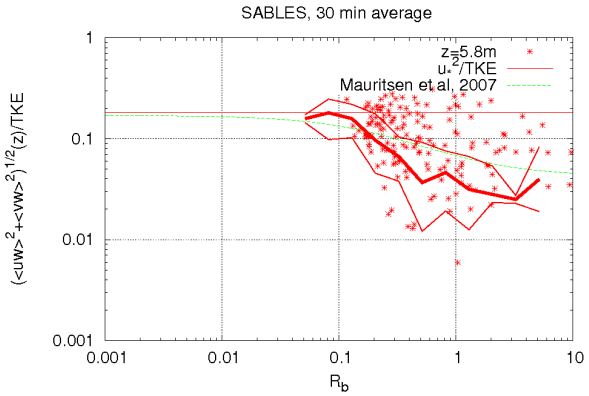

(a) $\frac{|\vec{\tau}|}{E_K}$ at $z = 5.8m$

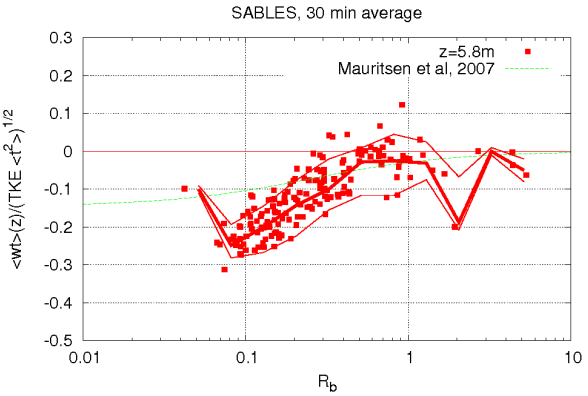

(b) $\frac{\overline{w'\theta'}}{\sqrt{E_K \overline{\theta'^2}}}$ at $z = 5.8m$

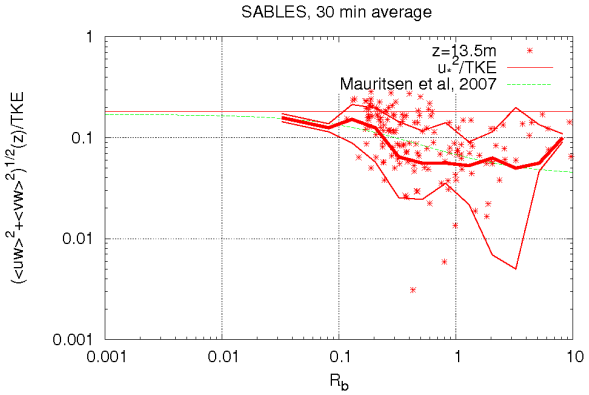

(c) $\frac{|\vec{\tau}|}{E_K}$ at $z = 13.5m$

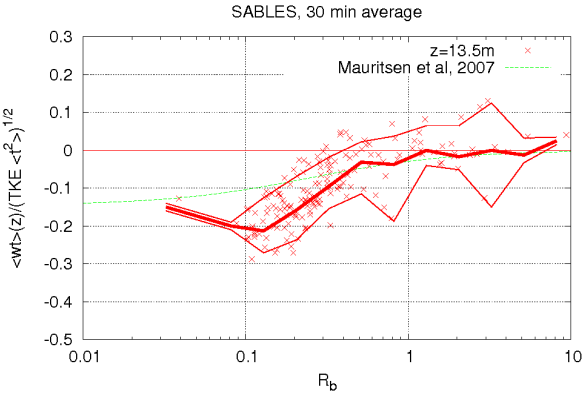

(d) $\frac{\overline{w'\theta'}}{\sqrt{E_K \overline{\theta'^2}}}$ at $z = 13.5m$

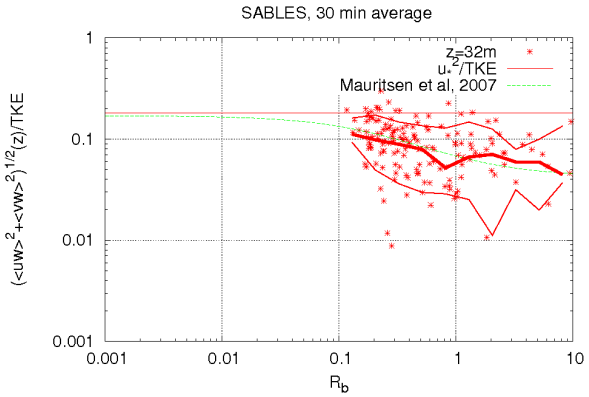

(e) $\frac{|\vec{\tau}|}{E_K}$ at $z = 32m$

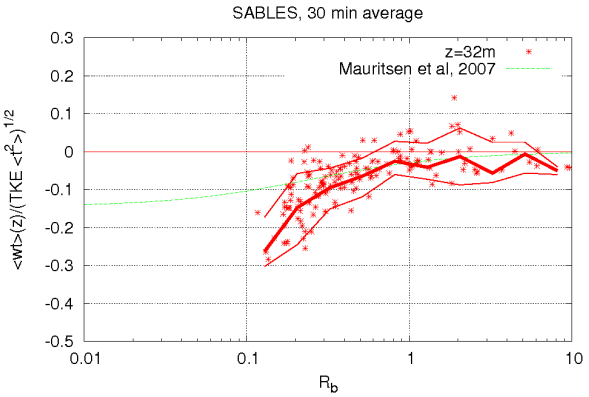

(f) $\frac{\overline{w'\theta'}}{\sqrt{E_K \overline{\theta'^2}}}$ at $z = 32m$

Figure 7: Non dimensional turbulent fluxes as functions of bulk Richardson number (Richardson number using finite-difference methods) at different heights. Red stars are data, the red straight lines are the near neutral surface value used by BOLAM, thick red line the median of the data, and the two thin red lines correspond to the 10% and 90% of the cumulant function of the data. Mauritsen functions correspond to eqs.(55). Data from CIBA site, Spain, are averaged over 30 minutes

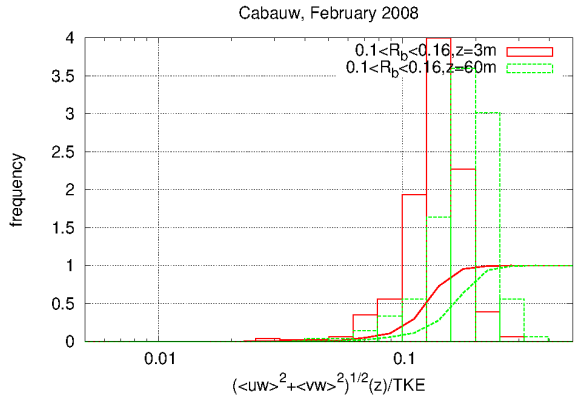

(a) $0.1 < Ri < 0.16$

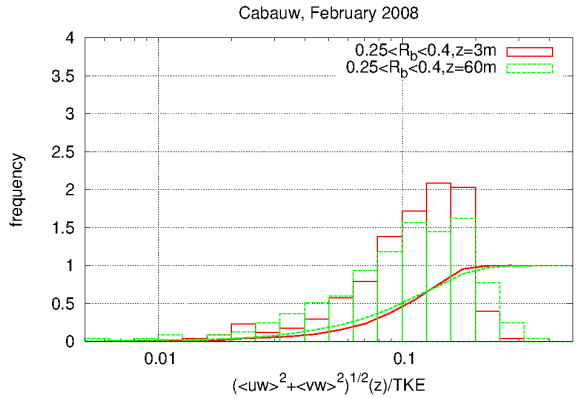

(b) $0.25 < Ri < 0.4$

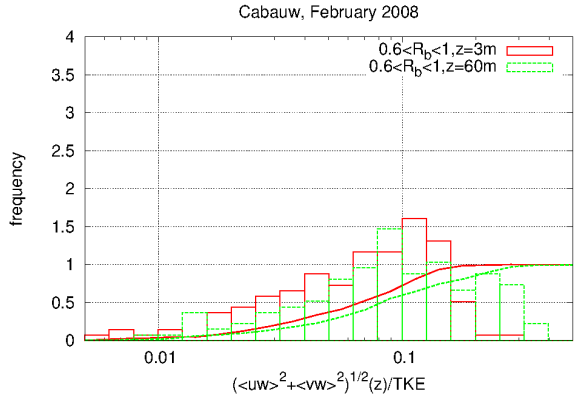

(c) $0.6 < Ri < 1$

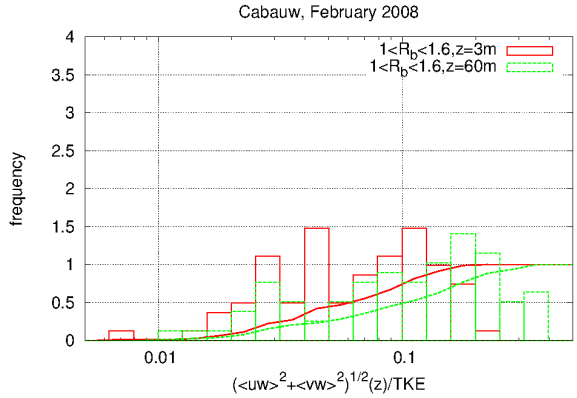

(d) $1 < Ri < 1.6$

Figure 8: pdfs of the ratio $\frac{|\vec{\tau}|}{E_K}$ for differents ranges of Ri and at differents altitudes. The cumulant functions are the lines between [0:1] frequencies. Data from Cabauw tower measurements of February 2008, Netherlands

5 Numerical Models

5.1 FakeBolam

The closure schemes described in chapter (4) are implemented on FakeBolam, a Single Column numerical Model (SCM) of the atmosphere, based on the BOLAM model. FakeBolam solves the set of equations (24), (25), (26) discretized on a staggered grid with a finite-difference scheme. The initialization of the model is made on a z-coordinate grid for simplicity, whereas the integration is performed on σ-coordinate for consistency with the BOLAM model. The transformation from z-coordinates to σ-coordinates is made using hydrostatic equation.
The time integration is performed using the splitting of the operators: the Coriolis terms are integrated with a simple forward Euler, while the vertical diffusions are integrated with a fully-implicit scheme which ensures inconditional stability of the integration (see i.e. Press et al., 1992, Numerical recipes in FORTRAN).
The vertical gradients are computed using a centered difference method, from here the necessity to use a staggered grid. The mean quantities are defined on integer levels, whereas turbulent fluxes, TKE, mixing length *etc* are defined on semi-integer levels (where the gradients are evaluated).
At the bottom, a free-slip boundary condition is imposed for horizontal velocity components on the integer levels, while the temperature boundary condition is defined on the half-integer levels in terms of skin temperature θ_{skin}, which is prescribed as a function of time. At the top, a zero-flux condition is imposed.
A schematic picture of the scheme is showed in figure 9 using z as vertical coordinate. It should be noted that the index of the levels starts from the top of the integration domain (denoted with *ntop*), and it increases towards the ground (with last level *nlev* for integer levels and $nlev+1$ for half-integer) because the σ-coordinate used during the integration increases downwards.

5.2 1D model vs 3D model

Testing the predictions of our 1D model is not immediate: comparing them with experimental measurements of vertical profiles is not easy. The difficulties arise from the assumptions made in the 1D model, since it is developed in order to isolate and study

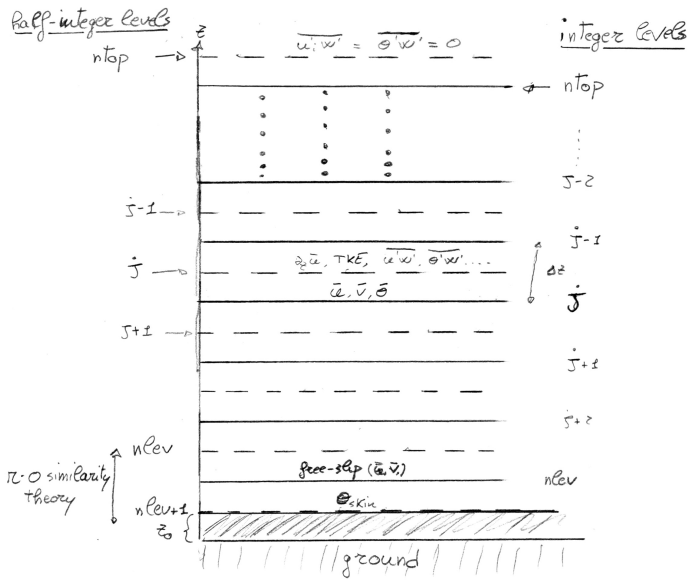

Figure 9: Schematic picture of FakeBolam vertical discretization and boundary conditions.

only the effect of turbulence closure in the evolution of the flow. On the other hand, this is a considerable limit for the comparison with the experimental data: the latter, even in the most idealized case, are always "polluted" by other processes, i.e. large scale motions or coupling effects of the ground with the atmosphere .
Thus, at this point, the issue is to compare the higly idealized results with something else equally idealized, which conversely is more similar to the real world than a 1D model. We shall follow the usual testing approach made in literature (i.e. Cuxart et al. (2006),Sorbjan (2012)), comparing the predictions of the 1D models with 3D predictions of a Large Eddy Simulation (LES) .

5.3 The LES approach

A Direct Numerical Simulation (DNS) of atmospheric flows is still not possible: It means to resolve all the turbulent eddies, from the dissipative scale η to the largest scale l_s, for instance $l_s \sim 300m$ in the atmosphere. The ratio of these two length scales, using

Kolmogorov theory, is (Garratt, 1992):

$$\frac{l_s}{\eta} \sim Re^{3/4} \tag{74}$$

For a typical boundary layer flow $U \sim 1m/s \Rightarrow \ Re \sim 10^7 \ \Rightarrow l_s/\eta \sim 10^5$. Therefore, the minimum length of eddies we should resolve is $\eta \simeq 1mm$, which would mean at least 10^{15} grid points for a 3D numerical simulations! That is the reason why DNS are possible only for low Reynolds number flows.

Therefore the basic idea of Large Eddy Simulations, as the name suggests, is to solve directly the largest eddies, which are the most energetic eddies, and to parametrize the smallest ones with some physical assumption. It should allow us to simulate even high Reynolds number flows, without loosing too many details.
In practice, what is usually done with isotropic grids, is to define a model representing the action of scales smaller than the grid size (see i.e. Compte et al., 1993). This separation is made applying a spatial low-pass filter of width Δx, the grid size, which allows to separate the flow in a filtered field $< \phi >$ and a sub grid scale (SGS) field ϕ'. The resulting filtered equations have a similar form of RANS equation (7); for example, for filtered momentum equation:

$$\begin{gathered} \frac{\partial}{\partial t} < u_i > + < u_j > \frac{\partial}{\partial x_j} < u_i > = \\ \frac{1}{<\rho>} \frac{\partial}{\partial x_i} < p > + g\delta_{i3} + \epsilon_{ij3} f < u_j > + \nu \frac{\partial^2}{\partial x_j^2} < u_i > + \frac{\partial}{\partial x_j} T_{ij} \end{gathered} \tag{75}$$

The term T_{ij} represents the sub-grid stress tensor formally similar to Reynolds stress tensor (9):

$$T_{ij} \equiv < u_i u_j > - < u_i >< u_j > \tag{76}$$

That should be parametrized with some closure.
The LES approach is similar in *form* to Reynolds decomposition and average, but have a deep conceptual difference: the filtered field $< \phi >$ is random inhomogeneus and unsteady even though the field is statistically homogeneus and steady. $< \phi >$ is a random field itself, not the first moment of a random field, as in RANS (Tampieri, 2011).
In the limit of Δx "big", the predictions of a LES converge in some sense, to the mean

(ensemble) flow of a RANS (Compte et al., 1993). The question which should arise is: How much is "big" ?
"Big" would mean with a dimension comparable to the size of energy-containing eddies. Here the problems of LESs in stably stratified flows arise.
As exposed in the introduction (1.2), in stable conditions the size of energy-containing eddies is highly reduced in respect with eddies in neutral or convective situations. Then, in order to have little influence of SGS model, LES in stably stratified flows must be at very high resolutions (Mason and Derbyshire, 1990). From previous works of Beare et al. (2006) (see also Beare and Macvean, 2004), we may assert that in weakly and moderate SBL in order to obtain a reasonable LES, vertical grid resolution should be less than 6.25 meters.

5.4 ARPS model

The Advanced Regional Prediction System (ARPS) is a three dimensional, non-hydrostatic compressible LES code used for small scale atmospheric flows. It is explicitely developed to work between regional and micro-scale, for boundary layer studies. A description of the model, the system of equations which solves, and the numerical scheme adopted by the model, are issues beyond the scope of this work, and could be found in great details in Xue (2000), Xue (2001). We only focus on the turbulence model used for the parametrization of sub grid scale eddies, and the parametrization of surface fluxes.

5.4.1 Parametrization of SGS eddies

For the parametrization of sub grid scale turbulence an eddy-viscosity model is used, equal in form to equation (31), which links the SGS motion with filtered variables. For the computation of turbulent eddy viscosity K_m, the same TKE-l scheme described in (3.3.2) is used with the main difference in the formulation of the mixing length which in isotropic grid is written, for stable conditions, as follows:

$$K_m \equiv 0.1\sqrt{E_k}l \qquad l = min(\Delta z, l_b) \tag{77}$$

where Δz is the grid spacing, and $l_b \equiv 0.76\sqrt{E_k}/N$, the buoyancy length scale (Moeng,

1984). This definition of mixing length takes into account the possible reduction of SGS eddies due to strong stability. The heat turbulent diffusion coefficient is computed using the turbulent Prandtl number:

$$Pr_t \equiv max(1/3, (1 + 2l/\Delta z)) \;\Rightarrow\; K_h = K_m/Pr_t \tag{78}$$

Dissipation of TKE is parametrized with K41 as (49), with costant $c_\epsilon = 3.9$ at the lowest model level (near the ground) and $c_\epsilon = 0.93$ above (see Deardorff, 1980) .

Surface stresses are parametrized as usual with Monin-Obukhov similarity theory and stability functions. ARPS defines only the stability functions for unstable conditions, and from them it computes stability functions for the other cases:

$$\begin{gathered}\psi_m = 2ln\left(\tfrac{1+\chi}{1+\chi_0}\right) + ln\left(\tfrac{1+\chi^2}{1+\chi_0^2}\right) - 2tan^{-1}\chi + 2tan^{-1}\chi_0 \\ \psi_h = 2ln\left(\tfrac{1+\eta}{1+\eta_0}\right)\end{gathered} \tag{79}$$

with

$$\begin{aligned}\chi &= (1 - 15\tfrac{z}{L_{MO}})^{1/4} \qquad & \chi_0 &= (1 - 15\tfrac{z_0}{L_{MO}})^{1/4} \\ \eta &= (1 - 9\tfrac{z}{L_{MO}})^{1/2} \qquad & \eta_0 &= (1 - 9\tfrac{z_0}{L_{MO}})^{1/2}\end{aligned}$$

Unlike our 1D model, the calculation of Monin-Obukhov length scale L_{MO} is made using an analytical solution from Byun (1990) that allows to compute z/L_{MO} as a function of z and bulk Richardson number Ri_b. Hence it is possible to compute surface fluxes with the drag laws (i.e. Jimenez et al. (2012)):

$$\begin{aligned}u_*^2 &= C_u^2 U^2 \qquad & U^2 &= u^2 + v^2 \\ \theta_* &= C_\theta \Delta\theta \qquad & \Delta\theta &= \theta_{1st} - \theta skin\end{aligned} \tag{80}$$

In neutral conditions the drag coefficients C_u, C_θ are calculated using the z/L_{MO} analytical function for unstable cases with an extremely negative value of bulk Richardson number. From these neutral condition coeffients the stable case is computed:

$$\begin{aligned}C_u^{stable} &= C_u^{neutr}\left(1 - \tfrac{Ri_b}{Ri_c}\right) \\ C_\theta^{stable} &= C_\theta^{neutr}\left(1 - \tfrac{Ri_b}{Ri_c}\right)\end{aligned} \tag{81}$$

Where Ri_c is a critical bulk Richardson number, defined as $Ri_c \equiv 3.05$

6 Numerical results

6.1 Test case of a neutral boundary layer

The first series of simulations which have been done had the goal to test the behaviour of the two schemes A and B of table 1, which are explained in details in chapter 4.
The test is made on the setup already described by Weng and Taylor (2003) (see also Weng and Taylor, 2005).
The horizontal axis are aligned with the barotropic geostrophic wind with intensity $u_g = 10m/s\, v_g = 0$. No forcing is imposed during the simulation (in terms of a cooling rate of the ground), so $\theta_{skin}(t) = 285^oK$. The roughness length is set to $z_0 = 0.01m$ and the Coriolis constant $f = 1.39\,10^{-4}s^{-1}$.
The wind at the initial time is set constant with height and equal to the geostrophic wind:

$$u(z) = u_g\; v(z) = 0$$

Potential temperature profile at initial time is constant with height and equal to the skin temperature so

$$\theta(z) = 285^oK$$

In these conditions, a neutral Ekman-layer is expected to develop.
FakeBolam is integrated for 30 hours on a vertical grid of 400 points with constant resolution of $\Delta z = 5m$, which corresponds to a vertical domain of $2000m$.

Run	Scheme	Type	mixing length l^{-1} (stable case)	Pr_t	u_*^2/E_K
A	BOLAM "original"	TKE - l	$(\frac{1}{kz}+\frac{1}{l_0})\frac{1}{1+12\,Ri}$	$1+5\,Ri$	$cost = 0.17$
B	Mauritsen's scheme	TTE - l	$(\frac{1}{kz}+\frac{f}{c_f\sqrt{\tau}}+\frac{N}{c_s\sqrt{\tau}})$	$\frac{K_m}{K_h}$	$0.17(0.25+\frac{0.75}{1+4\,Ri})$
$C1$	BOLAM mod1	TKE - l	Averaging of the mixing length of run A	$1+5\,Ri$	$cost = 0.17$
$C2$	BOLAM mod2	TKE - l	$(\frac{1}{kz}+\frac{f}{c_f\sqrt{\tau}}+\frac{N}{c_s\sqrt{\tau}})$	$1+5\,Ri$	$cost = 0.17$
$C3$	BOLAM mod3	TKE - l	$(\frac{1}{kz}+\frac{1}{l_0}+\frac{N}{c_d\sqrt{E_K}})$	$1+5\,Ri$	$cost = 0.17$
$D1$	BOLAM mod4	TKE - l	$(\frac{1}{kz}+\frac{1}{l_0})\frac{1}{1+12\,Ri}$	$(1+(4\,Ri)^3)^{1/3}$	$0.17(0.25+\frac{0.75}{1+(4\,Ri)^2})$ (only at the bottom boundary)
$D2$	BOLAM mod5	TKE -l	$(\frac{1}{kz}+\frac{1}{l_0})\frac{1}{1+12\,Ri}$	$(0.85)^3+(4\,Ri)^3)^{1/3}$ $k_{vk}^{(m)}=0.4$ $k_{vk}^{(h)}=0.47$	$0.17(0.25+\frac{0.75}{1+(4\,Ri)^2})$ (only at the bottom boundary)

Table 1: Summarizing table of the different schemes used inside FakeBolam. For more details, or for the values of constants used, see the text

In figure 10.a and 10.b the time evolution of u_* and of the u-component of the wind at fixed height are showed for the period of integration. The transient evolution of u_* is different for the two schemes, but they converge to the same value $u_* \simeq 0.37m/s$ after a time $t \simeq 25hrs$. The wind u-component shows the same evolution, with a steady state reached around $t \simeq 25hrs$. Looking at the equation of momentum (24), (25), it means that a balance between Coriolis force and Reynolds stresses is reached in the lowest part of the atmosphere. In the upper part ($z = 1502.5m$) the situation is different: the wind of run A is still equal to the geostrophic wind, therefore nothing has happened at this altitude, while the wind of run B shows an oscillatory regime. The period of this oscillation $T \simeq 12.5hrs$ is equal to the period of the pure inertial oscillation $T_{inertial} = 2\pi/f \simeq 12.5hrs$ due to the Coriolis term in the equation of motion. This implies that in the run B also the upper part of the atmosphere has been slightly perturbated, allowing an inertial oscillation to develops and persists, since Coriolis term dominates, compared to the term of the stresses.

In figure 11.a, the vertical profiles of the wind are showed. Both the wind profiles show

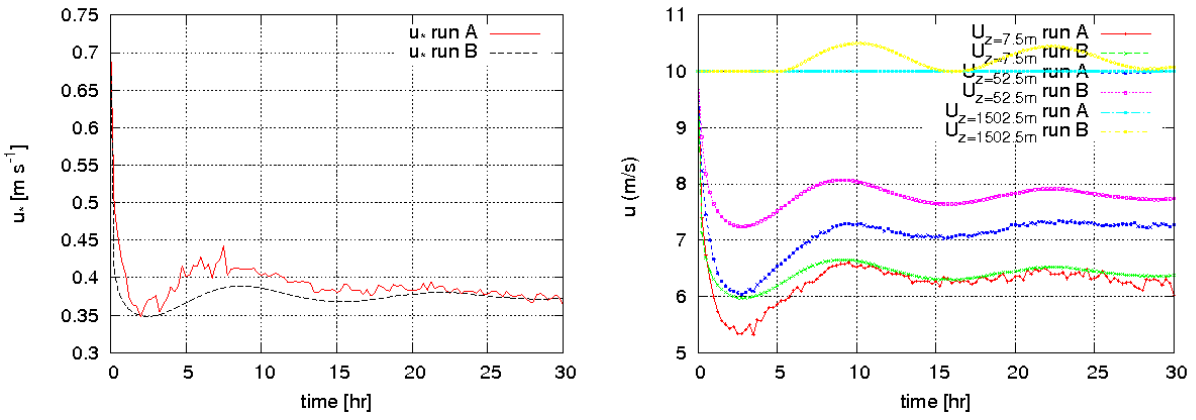

(a) (b)

Figure 10: Evolution in time of a) u_* and b) wind u-component of run A and B (see table 1) and ARPS, for the neutral simulation described in 6.1.

a Ekman-like profile with a rotation of the wind with height. Turbulent fluxes present a lot of noise in both simulations. The noise is due to the temperature profile, which is not exactly constant with height because numerical noise is present during the computation of potential temperature gradient. Such noise causes a fluctuation of potential temperature

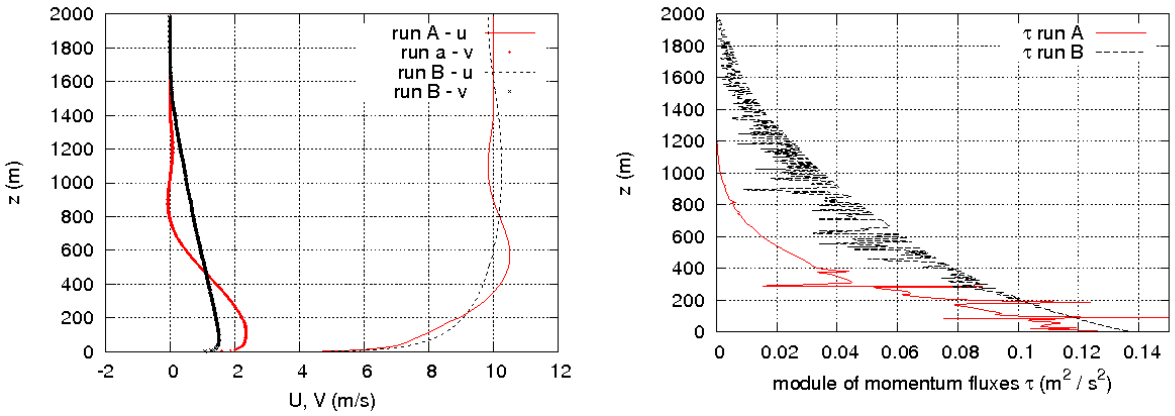

(a) (b)

Figure 11: Vertical profiles of a) wind components $\bar{u}, \bar{v}$ and b) the module of momentum flux, of run A, B, at the end of the neutral simulation ($t = 30hrs$) described in 6.1.

gradient around zero, thus a continuous changing in turbulent parametrization. This is clearly visible in the mixing length profile in figure 12.a, where for run A the mixing length is computed largely using the "non-local" convective formulation described in (4.4), which is completely different from Blackadar mixing length expected in near-neutral regimes. Being calculated using the mixing length, the same "non-physical" behaviour compares also in the eddy viscosity coefficient K_m. The mixing length of B works better, and here the strong noise is due to turbulent kinetic energy which is a function of Richardson number (figure 12). In this nearly-neutral regime, we expect that near the ground the surface layer theory is quite respected. In figure 13 we may observe that the wind profile for run B matches the neutral logaritmic profile expected in the first $200m$ from the ground. The same is showed for the diffusion coefficient, where the simulated K_m matches the surface layer value $K_m^{sfc} = kzu_*$.

6.2 Averaging the mixing length

The first modification raised concerns about the mixing length formulation of run A. Mixing length is a "global" quantity, which represents the integral scale of the eddies. On the other hand, in the models we compute it using local quantities, without any memory of the vertical mixing at which they are submitted.
In order to consider this effect, we applied to the quantities, used in the mixing length

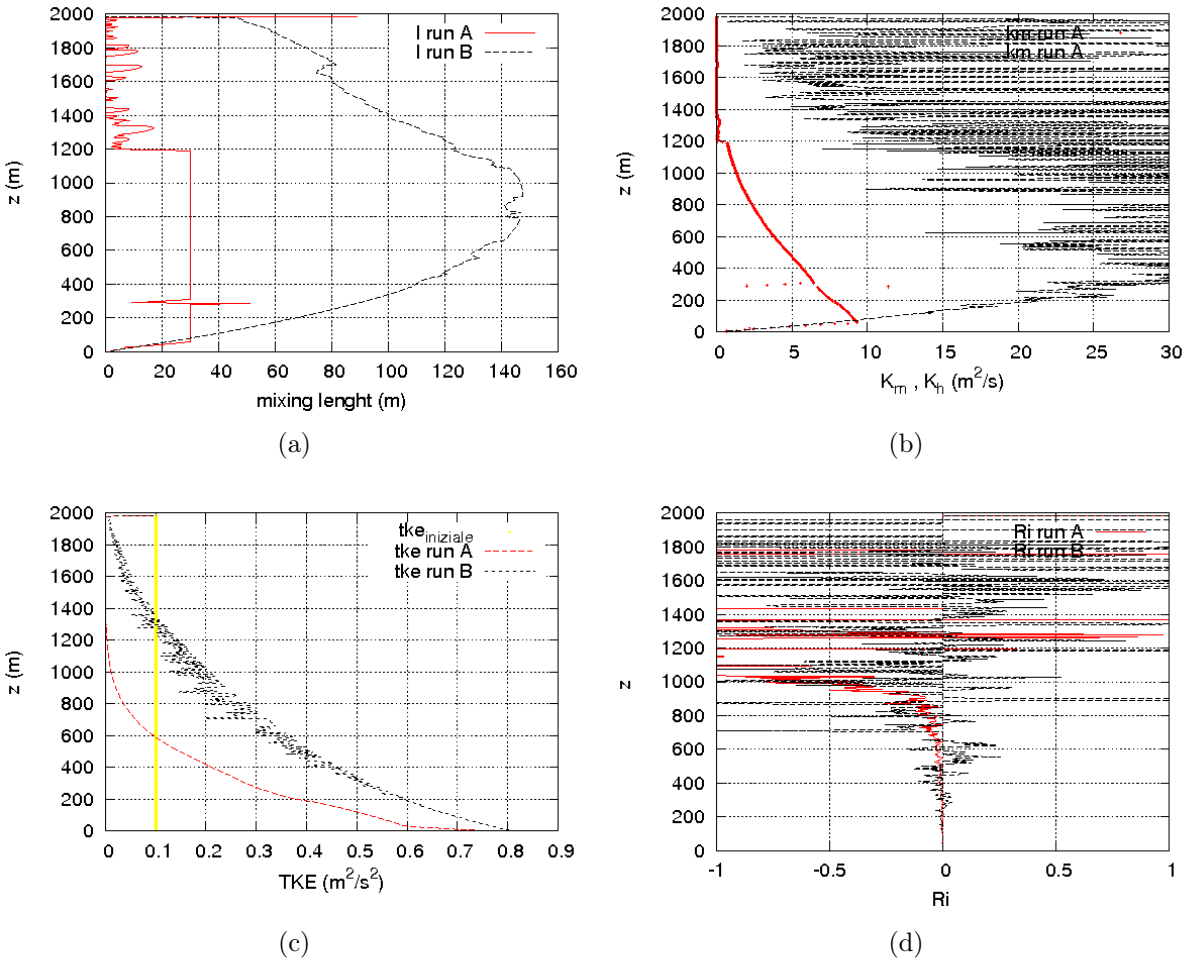

Figure 12: Vertical profiles of a) mixing length, b) eddy viscosity K_m, c) tke and d) Richardson number, of run A, B, at the end of the neutral simulation ($t = 30hrs$) described in 6.1.

computation, a mobile mean at each grid point, with averaging length l_{mean} equal to a multiple of the Blackadar mixing length at that altitude:

$$l_{mean}^{-1}(z) = 3\left(\frac{1}{kz} + \frac{1}{l_0}\right) \qquad l_0 = 100m \tag{82}$$

The average is weighted on the thickness of the single layers, hence in a non-linear grid the larger the layers, the more importance they have in the averaging.
The simulation of the previous neutral case with the averaged mixing length (run C1)

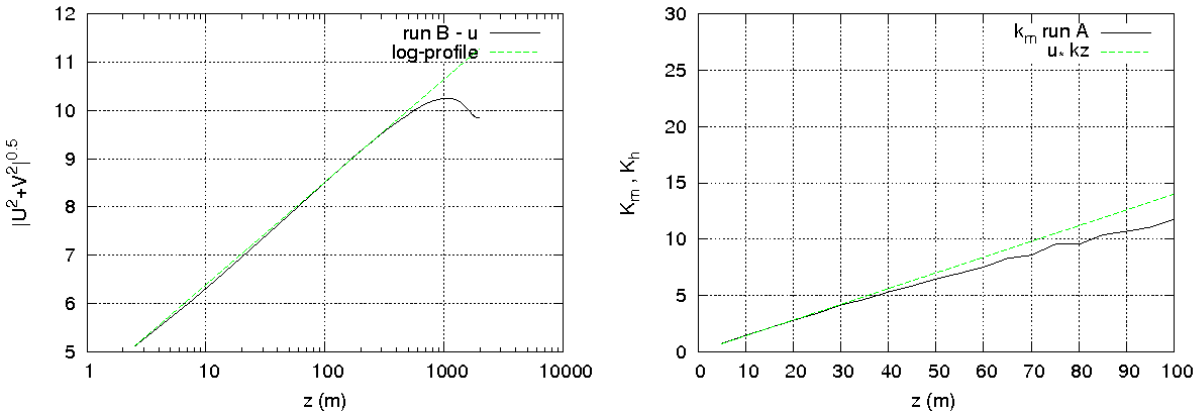

(a) (b)

Figure 13: a) Wind profile vs the log (theoretical) profile $\frac{u_*}{k}\ ln(\frac{z}{z_0})$ and b) eddy viscosity vs $K_m^{sfc} = kzu_*$ at the end of the neutral simulation ($t = 30hrs$) described in 6.1. The comparison is made only for run B

does not show large differences compared to run A. The noise in the gradient of potential temperature is reduced, but it is not exactly zero (figure 14.a). Hence the problem of the "choice" of the right turbulence parametrization remains (figure 14.b). This problem is soluble at this time only with the introduction of a neutral interval, in which the temperature gradient is numerically imposed to zero when it is less than a threshold value.

6.3 Case Studio: GABLS 1

The initial and boundary conditions for the comparison between FakeBolam and ARPS are based on a test-case deeply investigated in literature (Cuxart et al. (2006) ,Beare et al. (2006)) based on the measurement made during BASE on 1 october 1994 (see i.e. Kosovic and Curry (1999)), though adopting a slightly different wind at initial time.
The Coriolis parameter, as in the previous neutral case, is fixed to $f = 1.39\ 10^{-4}$. The roughness length $z_0 = 0.1m$.
The initial wind profile is assumed barotropic and equal to the geostrophic value, aligned

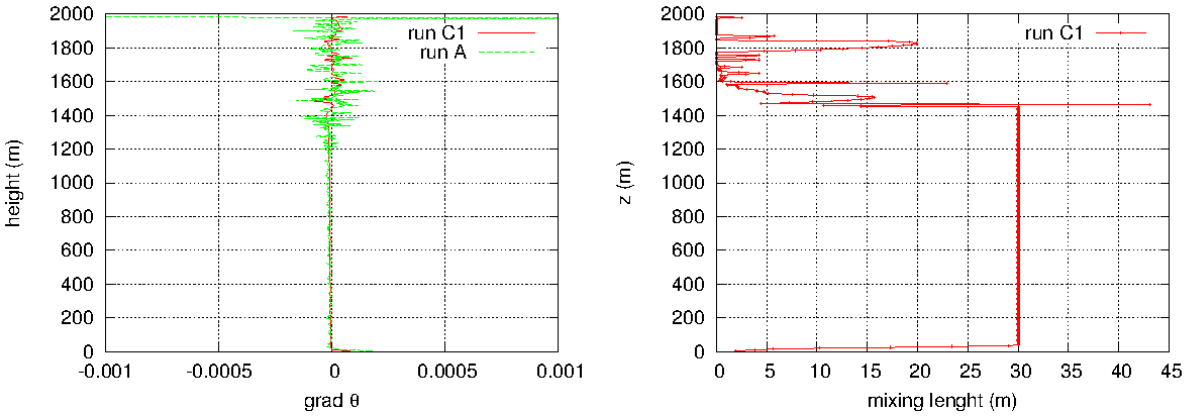

(a) (b)

Figure 14: Vertical profiles of a) potential temperature gradient, b) filtered mixing length of run C1, at the end of the neutral simulation ($t = 30hrs$) described in 6.1

with our reference system:

$$\left\{ \begin{array}{cc} \bar{u}(z) = u_g = 8m/s & z > 0 \\ \bar{v}(z) = v_g = 0 & \end{array} \right\} \tag{83}$$

Potential temperature profile is initialized with a shallow mixed layer capped with a weakly stable layer (with lapse rate equal to adiabatic lapse rate):

$$\left\{ \begin{array}{cc} \bar{\theta}(z) = 265\,K & 0 < z \leq 100m \\ \bar{\theta}(z) = 265 + 0.01\,(z - 100)\,K & z > 100m \end{array} \right\} \tag{84}$$

In order to stimulate turbulence, random potential temperature fluctuations of zero mean and amplitude 0.1 K is applied below $50m$:

$$\delta\theta(\vec{x}) = 0.1N(\vec{x})\,K \qquad 0 < z \leq 50m$$

where $N(\vec{x})$ is a white noise of amplitude 1^oK in (x, y, z) for ARPS, only in z for Fake-Bolam.

The stable stratification is developed by a prescribed, constant in time, cooling of ground temperature θ_{skin}. Radiative and soil schemes of ARPS are switched off, and the same

prescribed θ_{skin} is used:

$$z = 0 \quad \theta_{skin} = \theta(0) = 265 - \frac{0.25}{3600} t \, [K] \tag{85}$$

The models are run for 9 hours, in order to simulate a possible evolution of a stable night in high latitude regions.

For 1D models, a vertical domain of $400m$ is used, with a grid mesh of $\Delta z = 2m$, and a time step of $\Delta t = 5s$ (bearing in mind that the fully implicit scheme used for diffusion is unconditionally stable).
For ARPS, the domain size is set to $(400 \times 400 \times 400)$, and an isotropic grid is used with different resolutions: for our purpose, a "low" resolution grid with $\Delta = 3.125m$, and a "high" resolution grid with grid size $\Delta = 2m$ have been used. The determination of a suitable time step needs more investigation: ARPS is a fully compressible non hydrostatic model, and for the Courant-Friedrichs-Lewy (CFL) stability criterion (see i.e. Press et al., 1992, Numerical Recipes in Fortran) it must respect the inequality:

$$\frac{c|v|\Delta t}{\Delta x} \leq 1 \qquad c = 1 \tag{86}$$

CFL criterion is a necessary condition for stability, but it is not a *sufficient* condition: with $u \sim 10m/s$ the CFL criterion for grid size $\Delta = 3.125m$ should give $\Delta t = 0.3125s$, which does not work in our simulations.
For the simulation with grid size $\Delta = 3.125m$ the maximum time step permitting the stability of the simulation is $\Delta t = 0.06s$, which implies an (empiric) amplification factor $c \sim 5$.
For the simulation with grid size $\Delta = 2m$ the maximum time step permitting the stability of the simulation is $\Delta t = 0.02s$ which implies $c \sim 10$.
The comparison is made solely between one-dimensional model results and ARPS results, at a resolution $\Delta = 2m$.
In figure 15 is showed a schematic picture of the simulation at the initial time.

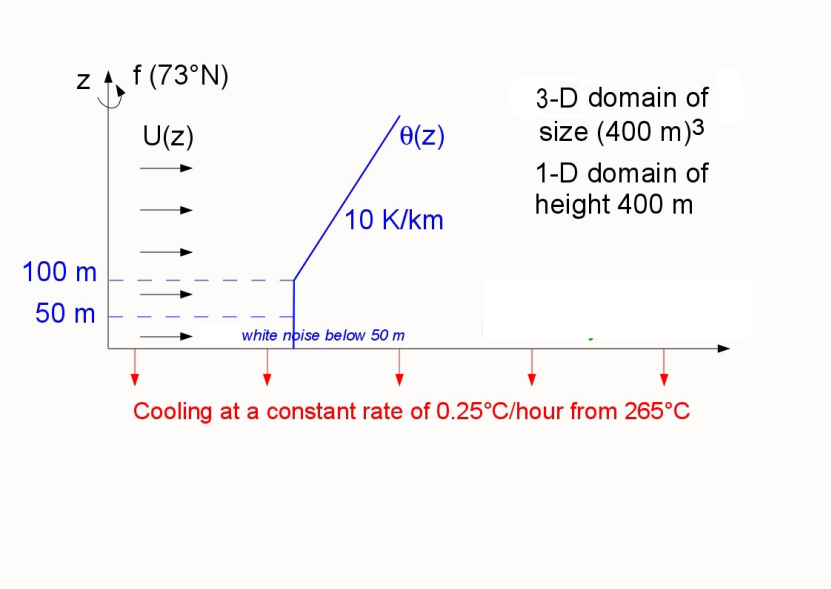

Figure 15: Schematic picture of the GABLS1-setup described in chapter 6.3

6.4 ARPS results

Being in horizontal homogeneus conditions, we may extract from the random field ϕ of our simulations (with $\phi = u, v, \theta\, etc..$) a horizontal mean field profile:

$$< \phi > (x, y, z) = \overline{< \phi >}(z) + < \phi >' (x, y, z) \tag{87}$$

where in this case $\overline{[\cdot]}$ is the averaging along horizontal domain. For economy from here on we shall define $< \phi > \equiv \phi$ for ARPS, saying implicitly that we are referring to the filtered fields, not to the total field.
The turbulent fluxes are the sum of the resolved-eddy fluxes and the sub grid scale eddy (SGS) fluxes: $\tau_{tot} = \tau_{res} + \tau_{SGS}$ where τ in this case represents a generic turbulent flux $\tau = \overline{u_i' \phi'}$. Using eq.(87) we can define the resolved turbulent fluxes as:

$$\overline{u_i' \phi} = \overline{(u_i - \bar{u}_i)(\phi - \bar{\phi})} \qquad \phi = u, v, w, \theta \tag{88}$$

A fundamental issue in LESs, is the the parametrization of the SGS fields in respect to the resolved parts. The larger this contribution is, the more the simulation will be similar to a RANS simulation.

In figure 16, the resolved and SGS turbulent fluxes (momentum and heat) for the

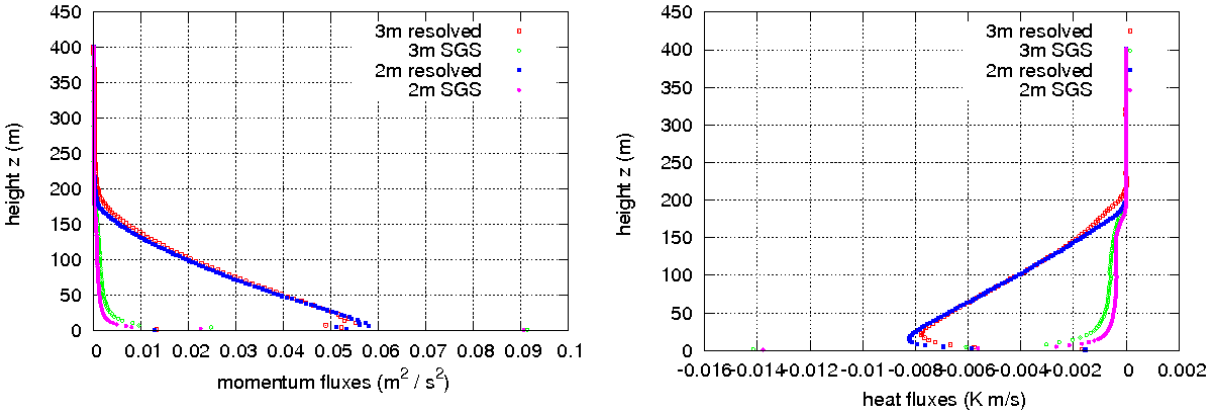

(a) (b)

Figure 16: Vertical profiles of the resolved and SGS parts of a) the module of momentum flux and b) the heat flux, for both the simulations made at different resolutions ($\Delta = 2m$, $\Delta = 3.125m$) of the case-studio described in 6.3. The quantities are averaged over the last hour of the simulation.

GABLS1 simulation are showed at different resolutions. The critical point for a LES is the size of the energy-containing eddies. The eddy size is not reduced only by stratification, but also by the presence of the ground, which bounds the size of the eddies (Mason and Derbyshire, 1990). In our simulations the SGS part of the fluxes is nearly always much smaller than the resolved part, starting to increase near the ground and finally becoming dominant only at the last two grid point for the highest resolution simulation.
An estimation of the vertical size of the most energetic eddies, could be done using the buoyancy length scale:

$$l_b = \frac{\overline{w'^2}^{1/2}}{N} \tag{89}$$

it is proportional to the displacement-scale of a fluid particle, if a balance between kinetic and available potential energy is assumed (Mason and Derbyshire, 1990).

In figure 17.a the buoyancy length scale computed using the resolved fields is showed. The vertical scale of resolved eddies is much larger than the grid size in the "central" part of SBL ($50 < z < 150$, where the contribution of SGS part is negligible), and becomes comparable with Δ only near the top of the boundary layer where the fluxes (figure 16) go to zero.

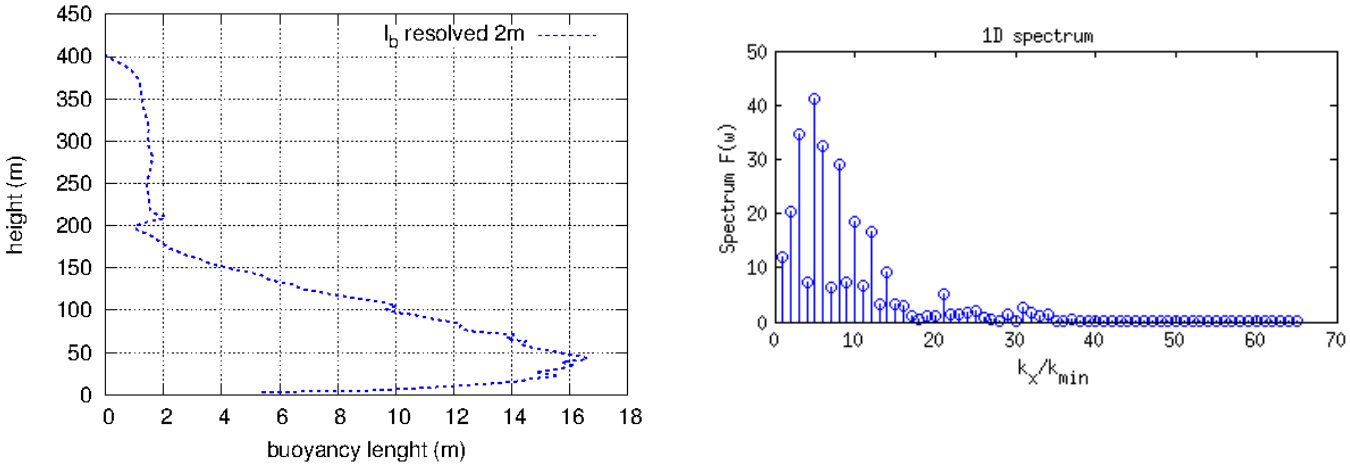

Figure 17: a) buoyancy length scale l_b defined in eq.(89) and b) 1-D spectrum along x-axis of the resolved $w'-$component of the wind at the end of the simulation ($t = 9hrs$) described in 6.3.

Therefore we may assert that for this weakly stable case, our LES simulations are reasonable in most part of SBL except near the boundaries.
Moreover, horizontal spectral analysis shows the strong anisotropy produced by the stable stratification on the eddy-size. If we assume the vertical scale of order $l_z \sim l_b \sim 10m$, horizontal spectrum in figure 17.b shows a peak around $k_i \simeq 5\, k_{min} = 5\, 2\pi/L$, where L is the dimension of the horizontal domain. Hence the horizontal length scale (injection energy-scale) of eddies may be computed:

$$l_h = \frac{2\pi}{k_i} \simeq 80m \tag{90}$$

and we may observe the anisotropic effect of stable stratification: $l_h \sim 100m \gg l_z \sim 10m$.

6.5 Comparison between 1D models and ARPS results

In figures 18.a and 18.b the time evolutions of u_* and θ_* are showed.
After a time $t \simeq 6hrs$ the u_* behaviour is similar for all the simulations, and it reaches a steady state with a value $u_* \simeq 0.3$. This means that the forcing near the ground of the momentum flux will be similar for ARPS, run A and run B, and then the behaviour of

the wind (which near the ground is driven by u_* by MO similarity). Due to the cooling of the ground θ_* starts to increase in absolute value, but unlike u_*, it does not reach a clear steady state. The value of the LES at the end of the simulation is larger than the 1D values, and, in particular, run A predicts a θ_* smaller (in absolute value) than run B, which would mean a surface heat flux smaller for run A than run B.

In figure 19.a and 19.b respectively, the vertical profiles for the mean quantities $\bar{u}, \bar{v}, \bar{\theta}$

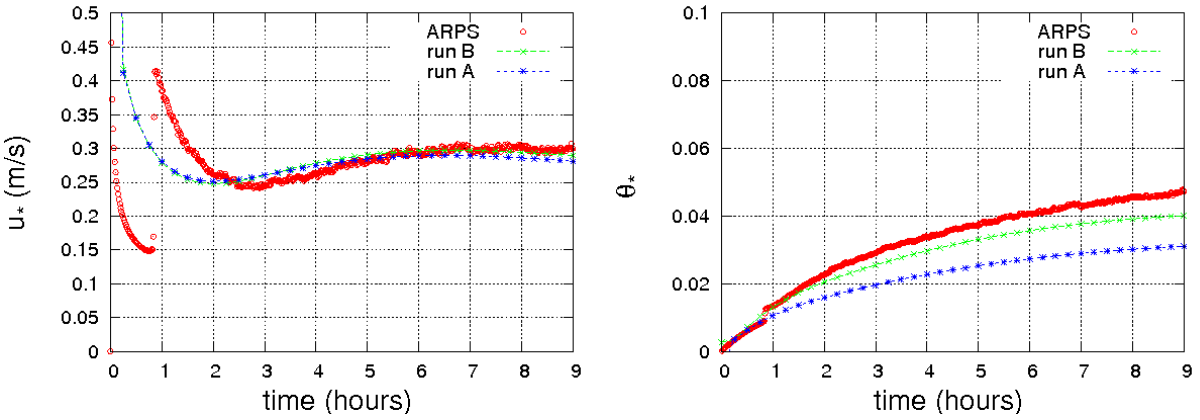

(a) (b)

Figure 18: Evolution in time of a) u_* and b) θ_*, of the run A, B (see table 1) and ARPS. In b), the sign of θ_* is inverted (θ_* is negative in stable situation) in respect to the output of the models.

are showed at the end of the simulations ($t = 9hrs$). As the analysis of u_* suggests the behaviour near the ground (up to $z \simeq 75m$) is similar for ARPS, run A and run B. All the runs present the characteristic supergeostrophic wind maximum of stable boundary layers, called low level jet (LLJ). LLJ is predicted by Nieuwstadt (1985) theory for a quasi-steady weak stable boundary layer, and it is also observed by experimental measurements (see i.e. Banta, 2008) in the higher part of SBLs. Run B shows a clear well-developed LLJ but at an altitude higher than the ARPS one. On the other hand, run A shows a wind profile too "spread" in the vertical, which is due to a large mixing of momentum still presents in the upper part of the BL.

Looking at the potential temperature profiles in figure 19.b, the LES simulation and run B are in accordance. The inversion layer expected with this setup (and also experimentally observed, (see Kosovic and Curry, 1999)) in the higher part of BL is reproduced

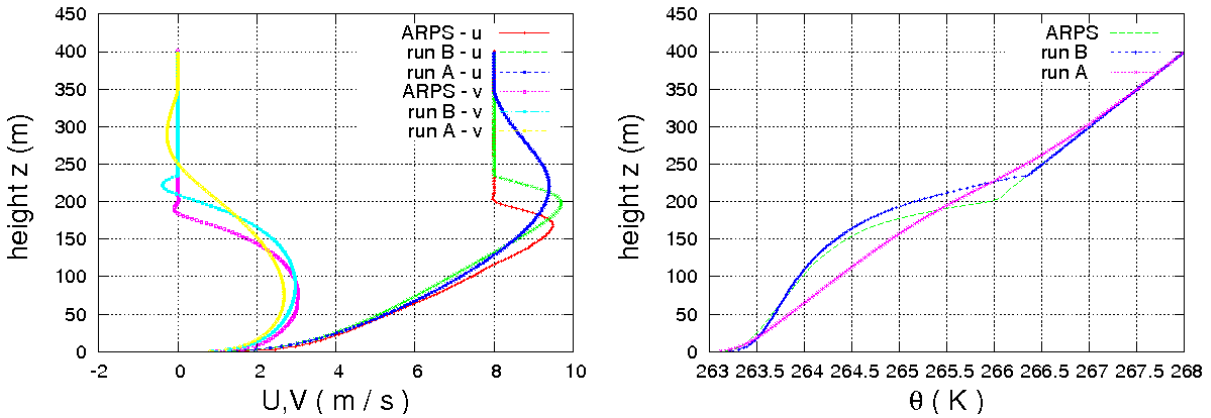

(a) (b)

Figure 19: Vertical profiles of a) wind components $\bar{u}$,$\bar{v}$ and b) $\bar{\theta}$, of the run A, B and ARPS at the end of the simulation ($t = 9hrs$) described in 6.3.

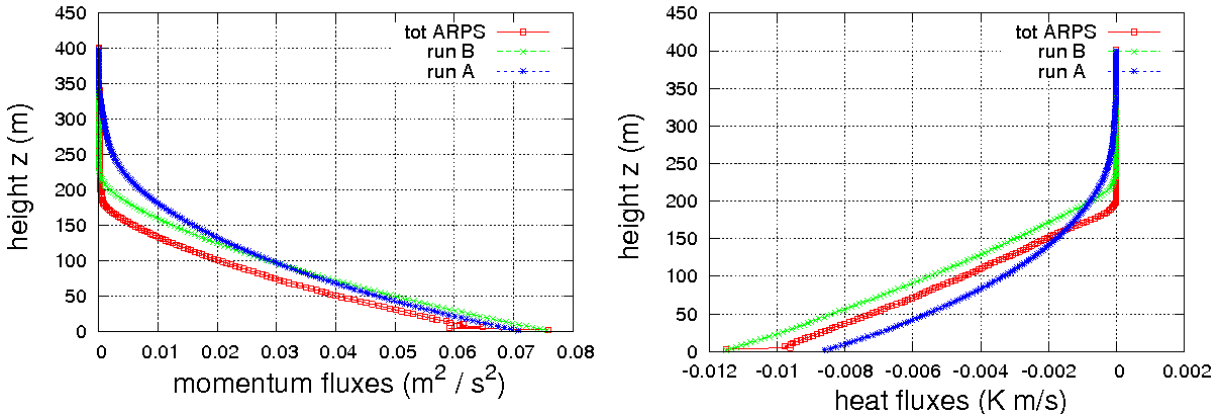

(a) (b)

Figure 20: Vertical profiles of a) module of momentum flux and b) of heat fluxes, of the run A, B and ARPS. For A, B the profiles are referred to the end of the simulation ($t = 9hrs$) described in 6.3. For ARPS the profiles are averaged over the last hour.

by both ARPS and run B. The second one overestimates the altitude of this inversion layer, compared to the LES. The altitude at which the temperature inversion develops is the same of the wind jet, which may mean that there is a link between these two phenomenons.

On the other hand, run A shows a potential temperature profile completely different from

the other two. This means that potential temperature mixing is highly underestimated in respect to the run B and ARPS: the cooling of the ground produces a downward heat flux (figure 9.b) which acts in order to mix the temperature of the layer, cooling the air above. The stronger the flux is, the smaller the potential temperature gradient will be in the central part of SBL. Looking at run A in figure 19.b, it seems that turbulent heat mixing is highly underestimated.

Figure 20 shows the vertical profile of fluxes (momentum, and heat) for the three simulations. As expected by potential temperature profiles, the heat flux (figure 20.b) for the run A is smaller than the other two simulations. Moreover, it could be noted that in both figures 20 the fluxes "suddenly" go to zero for the LES and run B, while for the run A the curves go down to zero in a smoother fashion, which makes it difficult to define clearly a SBL "height" (conventionally defined as the the altitude at which the module of momentum flux is 5% of u_*^2).

These different behaviours may be interpreted looking at the closure assumptions used by the one-dimensional schemes.

The vertical profiles of turbulent diffusion coefficients are showed in figure 21. It should

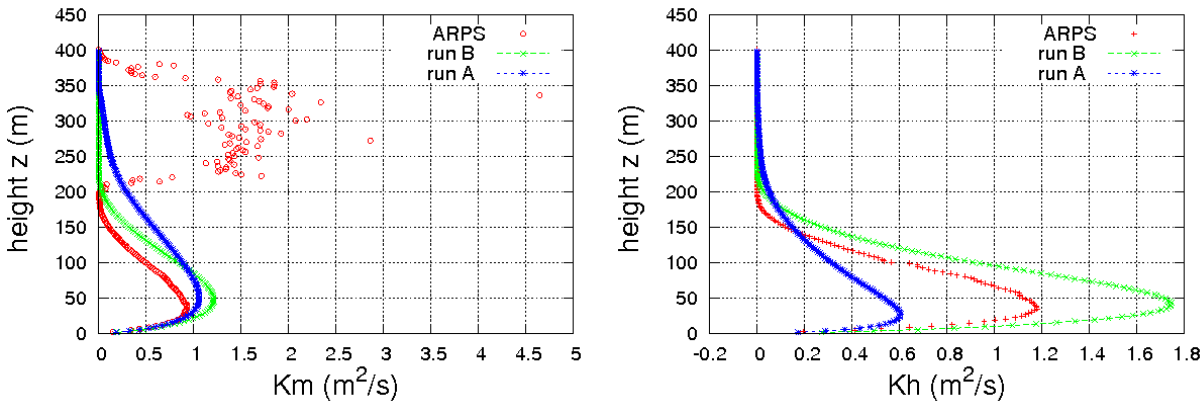

(a) (b)

Figure 21: Vertical profiles of a) eddy viscosity K_m and b)eddy diffusion K_h of the run A, B and ARPS. For A, B the profiles are referred to the end of the simulation ($t = 9hrs$) described in 6.3. For ARPS the profiles are averaged over the last hour.

be noted that the coefficients plotted for ARPS are "equivalent" diffusion coefficients, computed using resolved fluxes and the resolved wind vertical gradients.

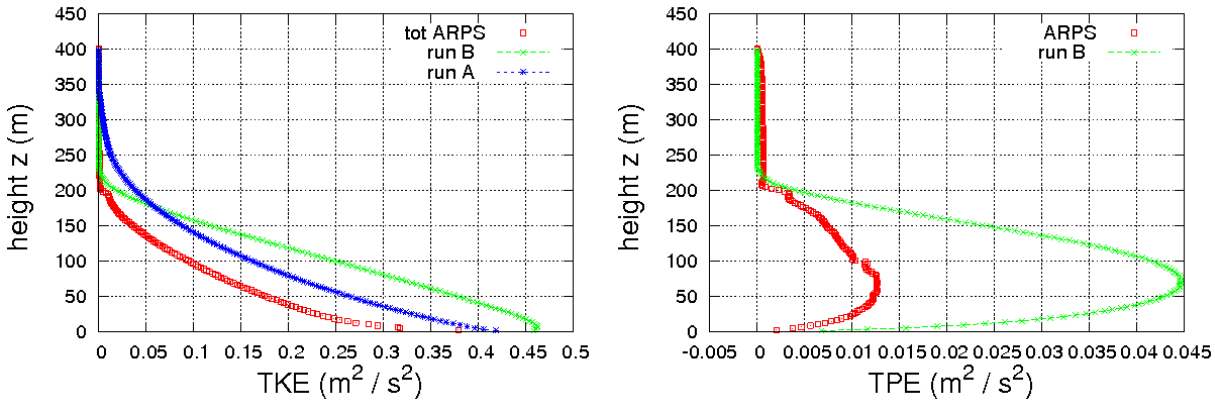

(a) (b)

Figure 22: Vertical profiles of a) TKE, b) TPE of the run A, B and ARPS. For A, B the profiles are referred to the simulation time $t = 9hrs$. For ARPS, the profiles are averaged over the last hour.

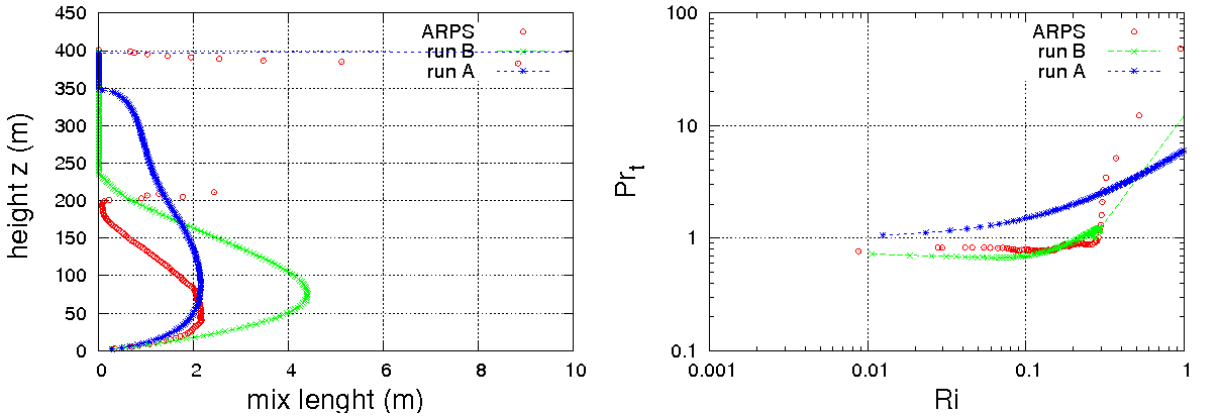

(a) (b)

Figure 23: Vertical profiles of a) mixing length and b) Prandtl number, of the run A, B and ARPS. For A, B the profiles are referred to the end of the simulation ($t = 9hrs$) described in 6.3. For ARPS, the profiles are averaged over the last hour.

The overestimation of momentum mixing at high altitude of run A is explained by K_m profile in figure 21.a. For run A the eddy viscosity K_m is different from zero up to $z \simeq 300m$, whereas for ARPS and run B it goes to zero around $z \simeq 150m$. This is mainly due to the mixing length (showed in figure 23.a) which does not feel the strong

effect of stratification and hence it is different from zero in almost the whole computational domain.
The heat diffusion coefficients K_h is highly underestimated by the run A compared to the LES result, whereas the K_h computed by B is too high. The latter one, is due to the parametrization of turbulent potential energy (showed in figure 22.b), which results too high compared to the resolved TPE computed by ARPS. It means that the simple interpolation formula used in equation (62) is too rough, and a more sophisticated formula should be used, in order to compute the right heat flux.
As far as run A is concerned, the computation of K_h depends on the Prandtl number formulation, which seems completely wrong compared to the LES (figure 23.b): Pr_t in run A grows quickly with the Richardson number, whereas the "resolved" Pr_t of the LES is almost constant in the whole range of Richardson number with a physical sense (up to $Ri \simeq 0.3$, which is the highest value of Ri reached in the BL). The result of the LES is in accordance with Zilitinkevich et al. (2013) argument, which says that in weak SBLs Pr_t grows very slowly with stability and it is almost constant, starts to increase with stratification only for $Ri > 1$, under very stable stratification.
The main effect of this Pr_t formulation is that turbulent mixing of heat is suppressed (even though K_m is in agreement with the LES in almost the whole of SBL), which is what we see in potential temperature profile in figure 19.b.

6.6 Modification of the BOLAM closure

The observed difficulties of BOLAM original scheme (A in table 1) in the previous simple case, suggest to try different parametrizations for some of the closure assumptions of A, in order to improve the results. Our modifications are summarized in table 1.

The first series of modifications which have been done concern the formulation of the mixing length (C2, C3 in table 1). The idea is to use a mixing length which does not suffer from the problems of the parametrization of A, and, furthermore, which may be extended continuosly to the convective case, resolving the problem of the near neutral cases.
Looking at the good results showed by the Mauritsen formulation (figure 23.a), we shall

try to use equation (60) in the BOLAM scheme (run C2).
We shall also attempt another parametrization, which is a modified version of the one developed by Duynkerke and Driedonks (1987), where the effect of the stability on the size of the eddies is counted using the buoyancy length scale l_b defined in eq.(89), where vertical velocity variance may be linked with the turbulent kinetic energy: $\overline{w'^2}^{1/2} = c_d E_K^{1/2}$. Hence the mixing length in stable condition is written:

$$l^{-1} = \left(\frac{1}{kz} + \frac{1}{l_0} + \frac{N}{c_d \sqrt{E_K}} \right) \qquad c_d = 0.36 \tag{91}$$

By surface layer measurements in near neutral conditions, (see i.e. Mellor, 1973) the ratio between the vertical velocity variance and the TKE should be $c_d \simeq 0.54$. However, in stable stratification this ratio is less than in the neutral case. In order to account for this reduction, Duynkerke and Driedonks (1987) calculated it far from the ground (where they suppose that the term (89) dominates in the interpolation formula (91), and Richardson numbers reach a constant values Ri_c, Ri_{fcrit}), using TKE equation (14) in steady condition:

$$c_d \simeq \left(c_e \frac{Ri_c}{1 - Ri_{fcrit}} \right)^{1/2} = 0.36 \tag{92}$$

The second series of modifications concern the Prandtl number formulation and the ratio u_*^2/E_K (run D1 in table 1). The latter modification follows from the analysis made in chapter (4.4), where we pointed out that the ratio u_*^2/E_K reduces with Ri faster than the Mauritsen function (55).Therefore we shall propose a new function t_τ which seems to work better against our data (figure 24):

$$\frac{u_*^2}{E_K} \equiv t_\tau = 0.17(0.25 + \frac{0.75}{1 + (4Ri)^2}) \tag{93}$$

This formulation for the ratio u_*^2/E_K are used in run D1 and D2 only as a boundary condition for the TKE, to compute it at the first level from the ground.
Prandtl number is a quantity more difficult to deal with. Experimental measurements of this quantity are difficult, because eddy diffusion coefficient $K_{m,h}$ are derived quantities from fluxes and gradients, which are often not measured at the same altitude. Hence, we shall use Pr_t derived by Zilitinkevich et al. (2013) which may be written as a function of Richardson number Ri. The Zilitinkevich formula is quite complicated, so we decided

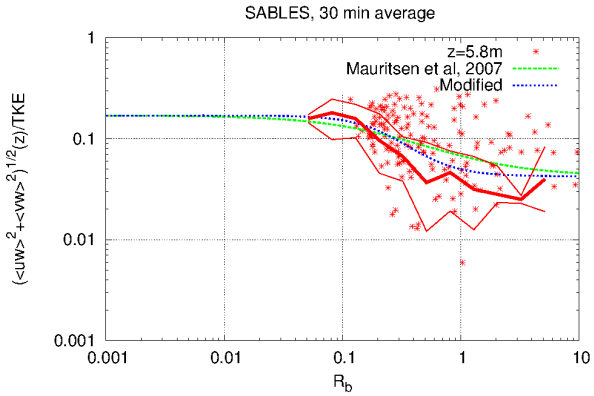

Figure 24: The Mauritsen function (55) (green line) and function $t_\tau(93)$ (blue line) against data at $z = 5.8m$ from CIBA site, Spain. As in figure 7 the thick red line are the median of the data, while the two thin red lines correspond to the 10% and 90% of the cumulant function of the data.

to use a simpler polynomial expression of Ri which fits well the original formula:

$$Pr_t(Ri) = (Pr_t(0) + (4\,Ri)^3)^{1/3} \tag{94}$$

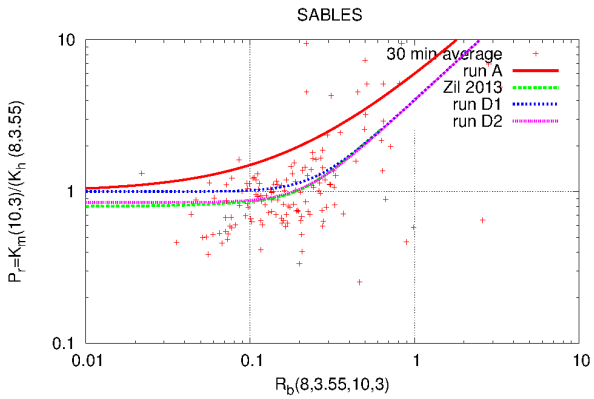

Figure 25: Different Pr_t formulation used in our simulations, plotted against experimental measurements from CIBA site, Spain. The numbers between brackets on the axis labels, are the altitude in meters at which the wind (for K_m) and the temperature (for K_h) are measured.

In figure 25 equation (94) with different values of $Pr(0)$ is showed against Zilitinkevich et al. (2013) curve, Pr_t used in run A, and experimental data (which show a large spread). Even though LES data in figure 23.b shows clear that $Pr_t(0) < 1$, in run D1 we use the same value of $Pr_t(0)$ of run A because changing the neutral limit value of Pr_t would mean to change also the surface layer parametrization. From the surface layer theory we know:

$$K_m^{sfc} = l_{sfc}/\phi_m(\frac{z}{L_{MO}}) \qquad K_h^{sfc} = l_{sfc}/\phi_h(\frac{z}{L_{MO}}) \tag{95}$$

Now, if we assume that the mixing length near the surface is the same for heat and momentum fluxes (as is made in run A, see chapter (4.5.3)), proportional to z by the Von Karman constant k_{vk} the Prandtl number at the surface is:

$$Pr_t(\frac{z}{L_{MO}}_{sfc}) = \frac{\phi_h(\frac{z}{L_{MO}})}{\phi_m(\frac{z}{L_{MO}})} \tag{96}$$

In our surface layer scheme (which is the same for all the run), in the limit $\frac{z}{L_{MO}} = 0$ the stability functions ϕ_m, ϕ_h are equal to one. Then the only possible value for Pr_{tsfc} in the neutral limit is $Pr_t(0) = 1$.
Hence, assuming the $Pr_t(0) \neq 1$ would imply that the mixing length near the surface is different for heat and momentum (as in the upper part of the BL), or equivalently that the Von Karman constant is different for heat and momentum. From ARPS simulation we may infer a value for $Pr_t(0) \simeq 0.85$ which would mean a *heat* Von Karman constant $k^{(h)}$:

$$Pr_t(0)_{sfc} = \frac{\phi_h(0)k^{(m)}z}{\phi_m(0)k^{(h)}z} \quad \Rightarrow \; k^{(h)} = 0.47 \tag{97}$$

that it is what it is used in run D2.

In figure 26, 27 some results of run C2 and C3 are showed, together with the original scheme (run A) and the LES. The setup of the simulation is always the case-studio described in 6.3. All the vertical profiles are the profiles at the end of the simulations.
The run C2 seems to work worse than A, compared to the LES. The "spread" of the velocity profile of C2 is larger than A, and it covers the whole computational domain. This means that momentum mixing is enhanced in respect to A. Looking at vertical profile of the mixing length (figure 27.b) the C2 mixing length is larger than A in all the BL,

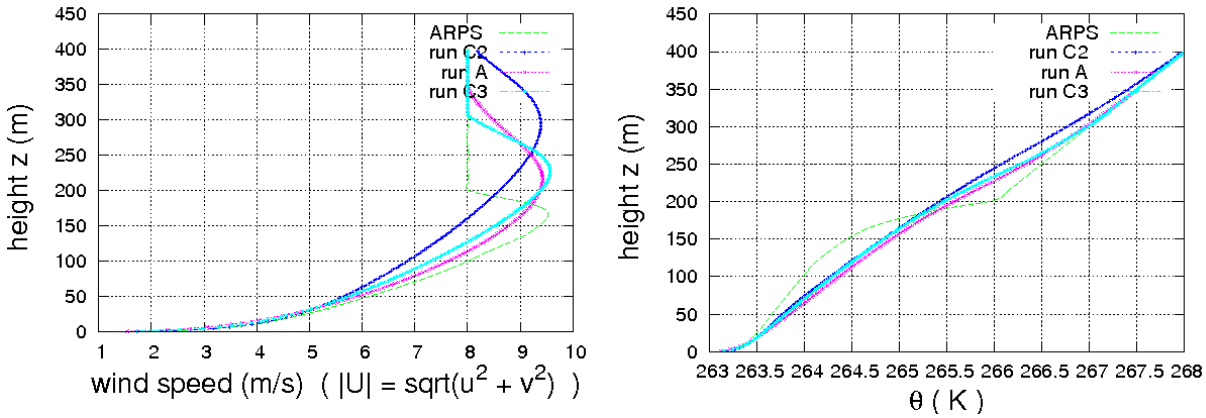

(a) (b)

Figure 26: Vertical profiles of a) the wind speed (module of the wind) and b) the potential temperature, for run C2, C3, A, ARPS, at the end of the simulation ($t = 9hrs$) described in 6.3.

which causes the enhanced mixing of momentum observed. The Mauritsen formulation used in C2 has the coefficient c_s tuned for the scheme B, which is not suitable for the scheme A.
Run C3 has a mixing length more similar to the LES, but globally there is not great improvement in the other quantities: i.e. in figure 27.a the TKE is showed, which is larger than run A.

In figure 28 the profiles of the mean quantities of run D1, D2 are showed, together with the original scheme A and ARPS.
The wind profile is unchanged, as it could be expected, and the largest differences are observable in the potential temperature profiles. To change the Pr_t formulation, has a great impact in the calculus of heat flux: the diffusion coefficient K_h (figure 30.c) is increased in respect to run A, and in run D1 it quite matches the K_h of the LES. Curiously, in run D2 the same $Pr_t(0)$ of the LES causes a larger K_h in respect with the K_h computed by the LES. These modified diffusion coefficients produce larger heat flux in run D1, D2 in respect to the original scheme A, and nearer the ARPS results.
The new Prandtl formulation does not lead to great modifications in TKE (figure 29.a). In figure 31.b the time evolution of the TKE at the first level from the ground ($nlev$)

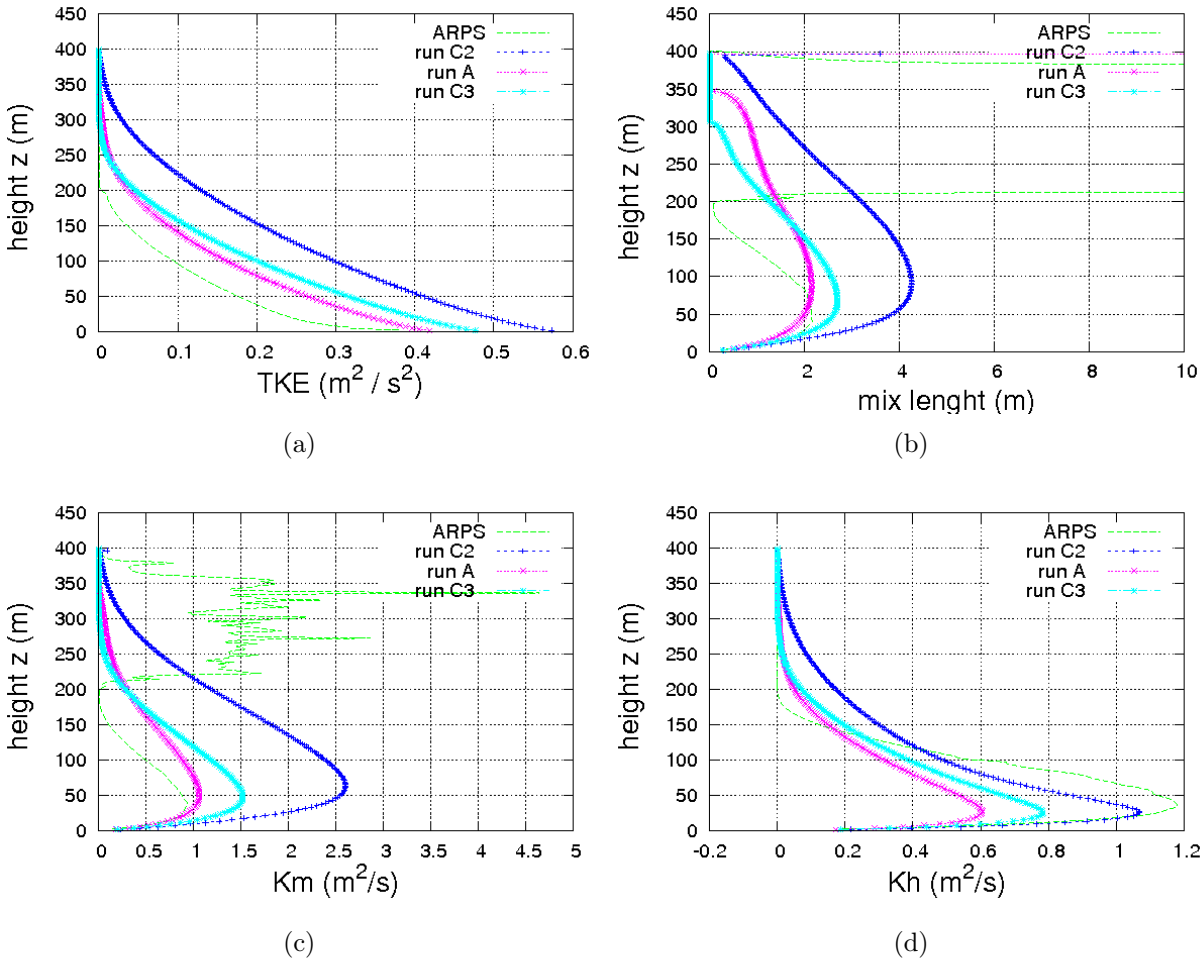

Figure 27: Vertical profiles of a) TKE, b) mixing length, c) eddy viscosity K_m, d) eddy diffusion K_h, for run C2, C3, A, ARPS. The setup is the same described in chapter 6.3. The profiles of C2, C3, A are referred to the end of the simulation time, $t = 9hrs$. The ARPS profiles are averaged over the last hour

is showed, only for the one-dimensional simulations. There is no effect of the boundary condition modification u_*^2/E_K, and the curves are practically equal.

The run D1, D2, show an increment of the θ_* (figure 31.b), which is more similar to the LES in respect to the original scheme A. This increment is a consequence of Pr_t modification, since by modifying the mixing in the "upper" part of the boundary layer, it has a feedback with the computation of surface layer values. In particular, looking at the potential temperature zoom in figure 28.c, in run D1 and D2 the temperature

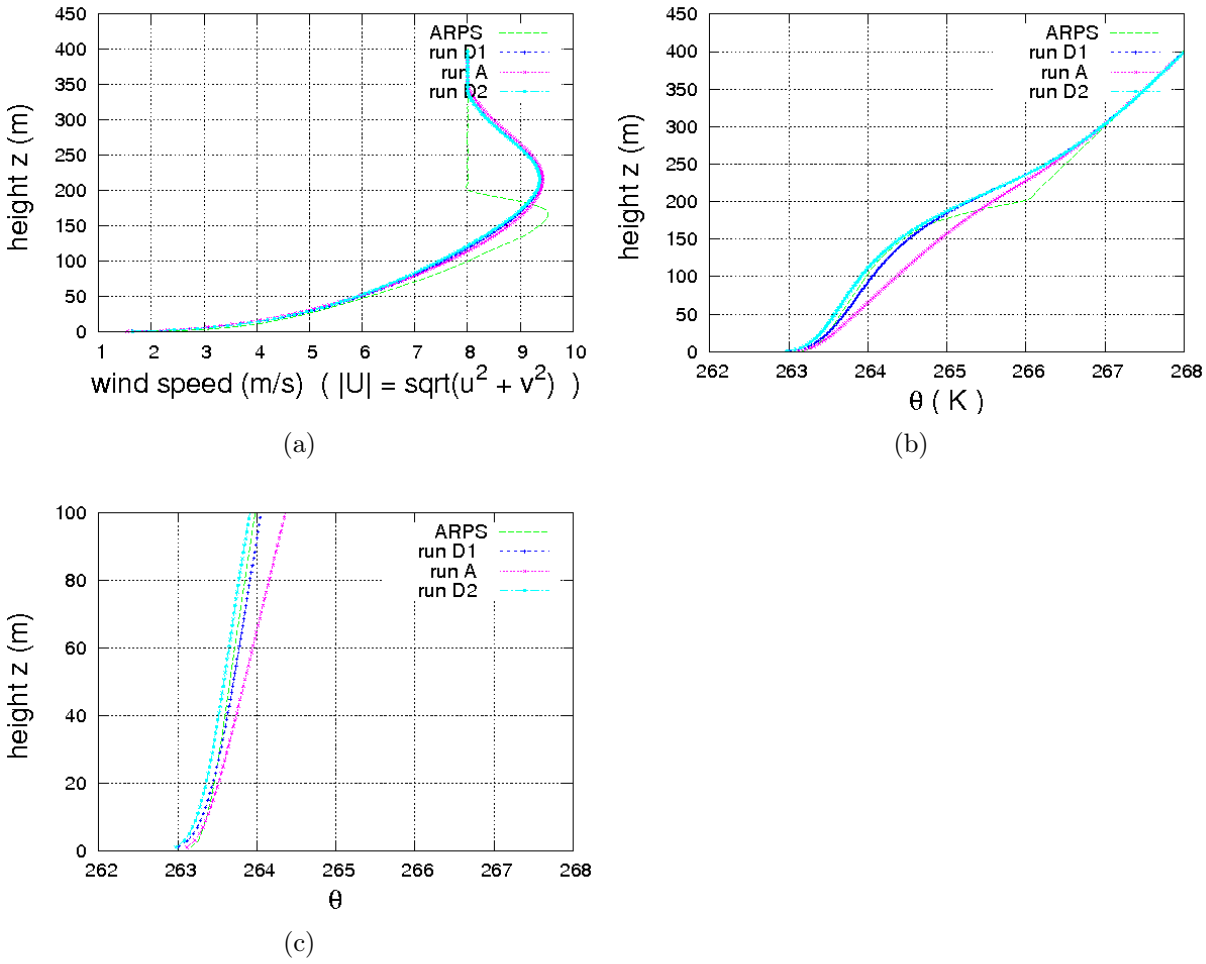

(a)

(b)

(c)

Figure 28: Vertical profiles of a) the wind speed (module of the wind), b) potential temperature and c) zoom of θ on the first $100m$ from the ground, of run D1, D2, A and ARPS at the end of the simulation ($t = 9hrs$) described in 6.3.

gradients between the ground and the first level from it, are lower than the run A. This means that there is more heat flux which acts in order to mix temperature, reducing the temperature gradient.

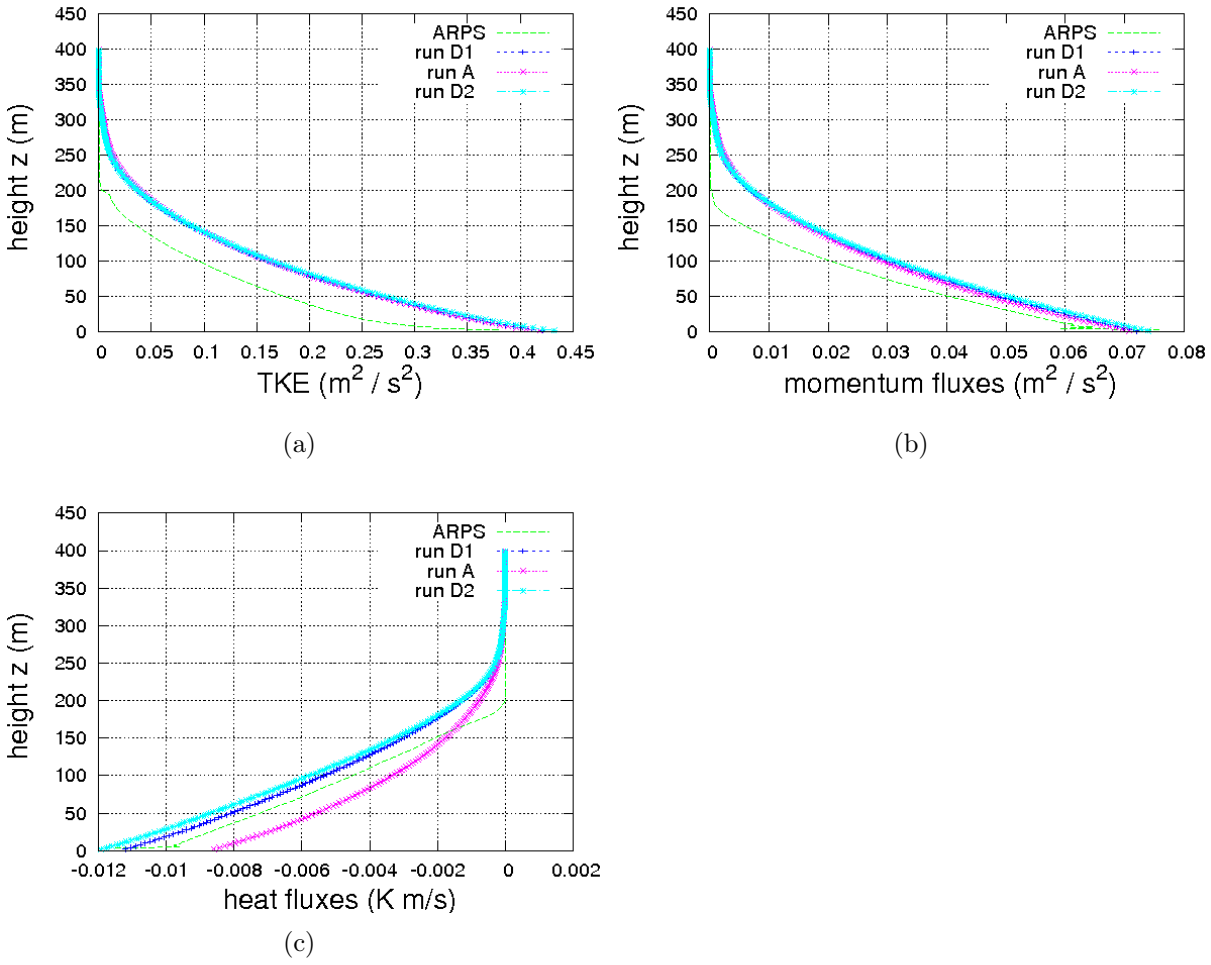

(a) (b)

(c)

Figure 29: Vertical profiles of a) TKE, b) module of momentum flux and c) heat flux of run D1, D2, A, ARPS. The setup is the same described in chapter 6.3. The profiles of D1, D2, A are referred to the end of the simulation ($t = 9hrs$).The ARPS profiles are averaged over last hour.

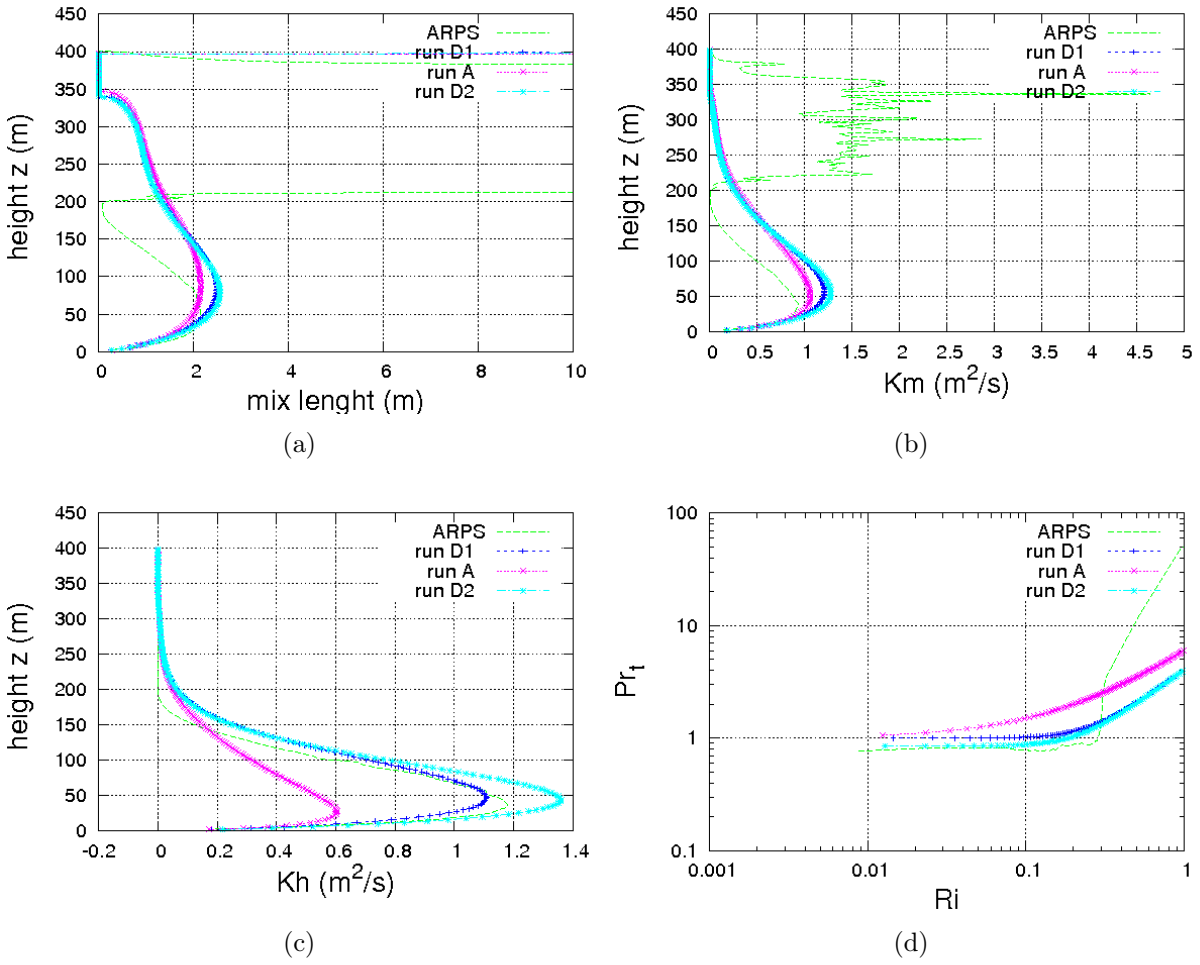

(a) (b) (c) (d)

Figure 30: Vertical profiles of a) mixing length, b) K_m, c) K_h, d) Pr_t of run D1, D2, A, ARPS. The setup is the same described in chapter 6.3. The profiles of D1, D2, A are referred to the end of the simulation ($t = 9hrs$).The ARPS profiles are averaged over last hour.

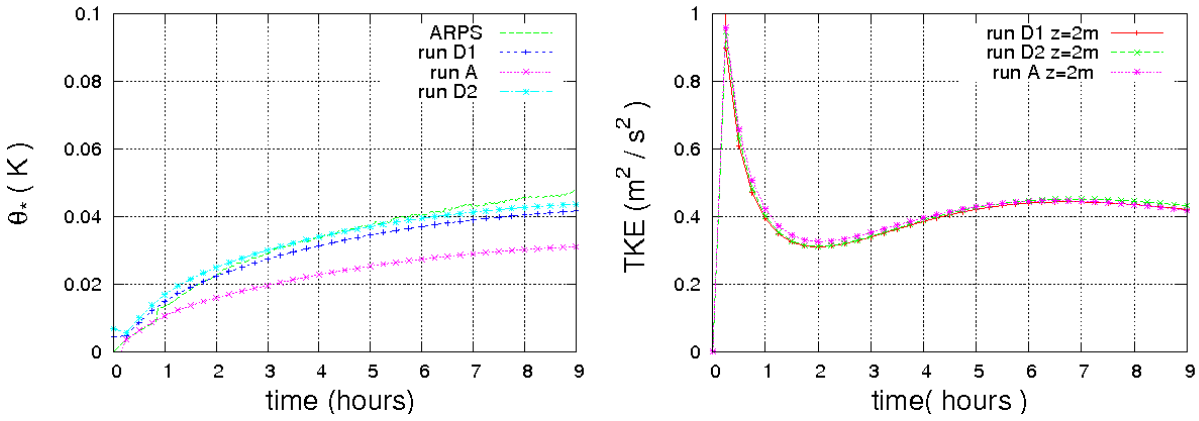

(a) (b)

Figure 31: Evolution in time of a) θ_* and b) TKE at the first level from the ground ($z = 2m$), of run D1, D2, A, ARPS. The TKE evolution is only of the one-dimensional models

7 Conclusions

In this work a study of Stable Boundary Layers has been performed.
For our purposes, we have developed a numerical code called FakeBolam:
FakeBolam is a Single Column Model (SCM) of the atmosphere devoted to boundary layer studies, particularly useful to test different closure of the Reynolds Average Navier Stokes (RANS) equations. The code is highly flexible, fast in the computation, and easy to use. As far as these qualities are concerned, it may be used beyond the scopes of this thesis work, rearranging it to other problems.

Inside FakeBolam, a TTE-l scheme and the BOLAM TKE-l scheme have been tested. For the comparison we also produced a three dimensional dataset using an high resolution LES code, ARPS, employed to assess the validity of FakeBolam predictions.
Our analysis of experimental data (from CIBA site, Spain and Cabauw tower, Netherlands) confirms the validity of the Mauritsen closure hypothesis for the ratio u_*^2/E_K as a function of Richardson number, but only for low Ri (< 1). For higher Ri the probability density functions of u_*^2/E_K of our data are almost flat. Hence, looking for a single value function of Ri for the ratio u_*^2/E_K could be questionable.
Looking at the results of our simulation made on GABLS1-setup, the TTE-l scheme overestimates turbulence mixing, for both momentum and heat compared to the LES results. This is a common problem of the RANS closure schemes, so well-known in literature. On the other hand, the results of TKE-l scheme are quite ambiguous: it highly overestimates momentum mixing, and at the same time it highly underestimates the heat mixing, compared to the LES. This fact is due to the Pr_t parametrization, which causes a suppression of heat mixing too fast with Ri.
Regarding this weakly stable case, we can affirm that the TTE-l scheme is in better agreement with the LES than the TKE-l scheme.
In order to improve the TKE-l scheme results, some original modifications of the scheme have been attempted, based on the previous data analysis and the LES results.
In particular we have seen that Mauritsen mixing length formulation is tuned for his TTE-l scheme: when it is introduced in the TKE-l scheme, the results are worse than the original scheme, compared to the LES.
The most serious problem of the TKE-l scheme is related to the parametrization of Pr_t,

which causes a strong underestimation of vertical mixing of potential temperature in respect to the LES. Changing the Pr_t with a formula in agreement with the LES results, produces a heat flux much more similar to the LES heat flux, which causes an improvement of the prediction of the potential temperature profile.
Nevertheless, the sole modification of the bottom boundary condition of TKE (using a formula similar to the one proposed by Mauritsen and Svensson (2007b)) does not lead to relevant difference between the model predictions.

The modification of Pr_t and u_*^2/E_K have been proposed as an improvement of BOLAM, and their influence inside the complete (fully 3-D) model have to be analyzed.
Future work could be:

- the development of a closure scheme based on two prognostic equations, one for the turbulent kinetic energy and one for the turbulent potential energy, following the work of Zilitinkevich et al. (2013).
- the implementation of a soil scheme in FakeBolam, which allows us to relax the hypothesis of an energetic balance between the ground and the air.
- the development of a mixing length formulation which both takes into account in the right way the reduction due to the stable stratification, and extends continuosly to the convective case.
- test a modified version of BOLAM scheme which takes into account the stability reduction to the ratio u_*^2/E_K at all levels. This must lead to an additional reduction of the turbulent mixing coefficients in stable condition because this ratio is implicitly used in the computation of $K_{m,h}$.
- test the performance of FakeBolam in convective (unstable) condition.

Acknowledgements

I would like to thank most sincerefully C. Yagüe and F. Bosveld for their concession of the experimental data from CIBA site and from Cabauw tower which have been employed in this work.

I would like to thank most sincerefully C. Chemel, who helped to configure and set up the ARPS code for the creation of the 3-D dataset.

Finally, I would like to thank most sincerefully prof. Francesco Tampieri. He did not teach me only everything I know about atmospheric boundary layer. He also taught me the methodological approach to problems that a researcher should have. At the end of this work, the latter seems me more fundamental than the former.

Ringraziamenti

I miei più sinceri ringraziamenti vanno:

Alla pieffe87 che mi ha accompagnato lungo tutto questo periodo di laurea magistrale. É stata una esperienza unica.

A domè e alla mia mamma. Vi ho già dedicato tutto il lavoro, non mi dilungo nei ringraziamenti!

Ai miei fratelli, che più o meno ci son sempre, e a dirla tutta se non era per Marcè dalla Francia indietro con tutti i miei averi non ci tornavo.

Ai massesi, che anche loro ci son sempre, e hanno quella capacità unica di farti sentire sempre la nostalgia di Casa.

Ad Andrea Dotta e Verdiana Vannini, che siete tanto lontani ma una mano riuscite sempre a darla.

Ad Alessandra, per essermi stata vicina sempre, per avermi dato forza anche quando avrei voluto lanciare il computer dal quarto piano. A pensarci bene, anche qualcosa di più di un grazie.

References

R. M. Banta. Stable-boundary-layer regimes from the perspective of the low-level jet. *Acta Geophysica*, 56(1):58–87, 2008.

R. J. Beare and M. K. Macvean. Resolution sensitivity and ascaling of large-eddy-simulations of the stable boundary layer. *Boundary-Layer Meteorology*, 112:257–281, 2004.

R. J. Beare, M. K. Macvean, A. A. M. Holtslag, J. Cuxart, I. N. Esau, J-C. Golaz, M. A. Jimenez, M. Khairoutdinov, B. Kosovic, D. Lewellen, T. S. Lund, Julie K. Lundquist, A. Mccabe, A. F. Moene, Y. Noh, S Raasch, and Peter P. Sullivan. An intercomparison of large-eddy simulations of the stable boundary layer. *Boundary-Layer Meteorology*, 118:247–272, 2006.

A.C.M Beljaars and A. A. M. Holtslag. Flux parameterization over land surfaces for atmospheric models. *J. Appl. Meteorol.*, 30:327–341, 1991.

A.K. Blackadar. The vertical distribution of wind and turbulent exchange in a neutral atmosphere. *J. Geophys. Res.*, 67(8), 1962.

D.W. Byun. *Journal Applied Meteorology*, 29:652–657, 1990.

P. Compte, M. Lesieur, and J.Z. Justin. *Computational fluid dynamics*. Elsevier Science ltd, 1993.

Felipe D. Costa, Octavio C. Acevedo, Jose' C. M. Mombach, and G. A. Degrazia. A simplified model for intermittent turbulence in the nocturnal boundary layer. *Journal of Atmospheric Sciences*, 68:1714–1729, 2011.

J. Cuxart, C. Yague, G. Morales, E. Terradella, J. Orbe, J. Calvo, A. Fernandez, M. R. Soler, C. Infante, P. Buenestado, A. Espinalt, H. E. Joergensen, J. M. Rees, J. Vila, JosÃ© Manuel Redondo, I. R. Cantalapiedra, and L. Conangla. Stable atmospheric boundary-layer experiment in Spain (SABLES 98): a report. *Boundary-Layer Meteorol.*, 96:337–370, 2000.

J. Cuxart, A. A. M. Holtslag, R. J. Beare, E. Bazile, A.C.M Beljaars, A. Cheng, L. Conangla, M. Ek, and F. Freedman. Single-column model intercomparison for a stably stratified atmospheric boundary layer. *Boundary-Layer Meteorol.*, 118:273–303, 2006.

J. W. Deardorff. Stratocumulus-capped mixed layers derived from a three-dimensional model. *Boundary Layer Meteorology*, 18:495–527, 1980.

A. Delage, P.A. Bartlett, and J.H. McCaughey. Study of soft night-time surface-layer decoupling over forest canopies in a land-surface model. *Boundary Layer Meteorology*, 103:253–276, 2002.

S. H. Derbyshire. Stable boundary-layer modelling: established approaches and beyond. *Boundary-Layer Meteorology*, 90:423–446, 1999a.

S. H. Derbyshire. Boundary layer decoupling over cold surfaces as a physical boundary instability. *Boundary-Layer Meteorology*, 74:19–54, 1999b.

P.G. Duynkerke and A.G.M. Driedonks. A model for the turbulent structure of the stratocumulus-topped atmospheric boundary layer. *American Meteorology Society*, 44:53–65, 1987.

R. P. Feynman, R. B. Leighton, and M. Sands. *The Feynman Lectures on Physics*, volume II. Addison-Wesley Publ. Co., London, 1969.

U. Frisch. *Turbulence*. Cambridge University Press, 1995. 296 pages.

J. R. Garratt. *The atmospheric boundary layer*. Cambridge University Press, 1992. 316 pp.

P. A. Jimenez, Jimy Dudhia, J. Fidel Gonzalez-Ruoco, J. Navarro, J. P. Montavez, and Elena Garcia-Bustamante. A revised scheme for the WRF surface layer formulation. *Monthly Weather Review*, 140:898–918, 2012.

A. N. Kolmogorov. The local structure of turbulence in incompressible viscous fluid for very large Reynolds numbers. *Dokl. Akad. Nauk SSSR*, 30:301, 1941.

J. Kondo, O. Kanechika, and N. Yasuda. Heat and momentum transfers under strong stability in the atmospheric surface layer. *Journal of Atmospheric Sciences*, 35:1012–1021, 1978.

B. Kosovic and J.A. Curry. A large eddy simulation study of a quasi-steady, stably stratified atmospheric boundary layer. *Journal of Atmospheric Science*, 57(1):1052, 1999.

L.D. Landau and E.M. Lifshitz. Fluid mechanics. 1987.

Larry Mahrt. Stratified atmospheric boundary layers. *Boundary-Layer Meteorol.*, 90: 375–396, 1999.

P. C. Mason and S. H. Derbyshire. Large-eddy simulation of the stably-stratified atmospheric boundary layer. *Boundary-Layer Meteorology*, 53:117–162, 1990.

T. Mauritsen and G. Svensson. A total turbulent energy closure model for neutrally and stably stratified atmospheric boundary layers. *Journal of Atmospheric Sciences*, 64: 4113–4124, 2007a.

T. Mauritsen and G. Svensson. Observations of stably stratified shear-driven atmospheric turbulence at low and high richardson numbers. *Journal of Atmospheric Sciences*, 64: 645–655, 2007b.

G. L. Mellor. Analytic prediction of the properties of strtified planetary surface layers. *J. Atmos. Sci.*, 30:1061–1070, 1973.

G. L. Mellor and T. Yamada. Development of a turbulence closure model for geophysical fluid problems. *Reviews of Geophysics and Space Physics*, 20(4):851–875, 1982.

C-H. Moeng. A large-eddy-simulation model for the study of planetary boundary-layer turbulence. *journal of the atmospheric science*, 41(13):2052–2062, July 1984.

A. S. Monin and A. M. Yaglom. *Statistical fluid mechanics*, volume I. MIT Press, Cambridge, 1971. 769 pp.

A.S. Monin and A. M. Obukhov. Basic laws of turbulent mixing in the ground layer of the atmosphere. *Trudy In-ta Theoret. Geofiz. AN SSSR*, 151:163–187, 1954. in Russian.

F. T. M. Nieuwstadt. The turbulent structure of the stable, nocturnal boundary layer. *J. Atmos. Sci.*, 41:2202–2216, 1984.

F. T. M. Nieuwstadt. A model for the stationary, stable boundary layer. In J. C. R. Hunt, editor, *Turbulence and diffusion in stable environments*, pages 149–220. Clarendon Press, Oxford, 1985.

S. Pope. *Turbulent Flows*. Cambridge University Press, 2000.

William H. Press, S. A. Teukolsky, W. T. Vetterling, and B. P. Flannery. *Numerical Recipes in FORTRAN*. Cambridge University Press, 2nd edition, 1992.

Z. Sorbjan. Gradient-based scales and similarity laws in the stable boundary layer. *Quarterly J. Royal Meteorol. Soc.*, 136:1243–1254, 2010.

Z. Sorbjan. A study of the stable boundary layer based on a single column k-theory model. *BoundaryLayer Meteorology*, 142(1):33–53, 2012.

E. A. Spiegel and G. Veronis. On the boussinesq approximation for a compressible fluid. *Astrophys. J.*, 131:442–447, 1960.

G. J. Steeneveld, B. J. H. van de Wiel, and A. A. M. Holtslag. Modelling the arctic stable boundary layer and its coupling to the surface. *Boundary Layer Meteorology*, 118:357–378, 2006.

R. B. Stull. *An introduction to boundary layer meteorology*. Kluwer Academic Publishers, 1988.

Francesco Tampieri. *Appunti sul corso di strato limite atmosferico e diffusione turbulenta*. 2011.

G.K. Vallis. *Atmospheric and oceanic fluid dynamics*. Cambridge University Press, 2006.

W. Weng and P. A. Taylor. On modelling the one-dimensional atmospheric boundary layer. *Boundary-Layer Meteorology*, 107:371–400, 2003.

W. Weng and P. A. Taylor. Modelling the one-dimensional stable boundary layer with an e-l turbulence closure scheme. *Boundary-Layer Meteorology*, 118:305–323, 2005.

J. C. Wyngaard. Modelling the planetary boundary layer- extension to the stable case. *Boundary Layer Meteorology*, 9:441–460, 1975.

J. C. Wyngaard. *Turbulence in the Atmosphere*. Cambridge University Press, 2010.

M. Xue. The advanced regional prediction system (arps) - a multi-scale nonhydrostatic atmospheric simulation and prediction model. part i: Model dynamics and verification. *Meteorology and Atmospheric Physics*, 75:161–193, 2000.

M. Xue. The advanced regional prediction system (arps) - a multi-scale nonhydrostatic atmospheric simulation and prediction tool. part ii: Model physics and applications. *Meteorology and Atmospheric Physics*, 76:143–165, 2001.

S. S. Zilitinkevich, T. Elperin, N Kleeorin, and I. Rogachevskii. Energy- and flux-budget (efb) turbulence closure model for stably stratified flows. part i: steady-state, homogeneous regimes. *Boundary-Layer Meteorology*, 125:167–191, 2007.

S. S. Zilitinkevich, T. Elperin, N Kleeorin, I. Rogachevskii, and I. N. Esau. A hierarchy of energy- and flux-budget (efb) turbulence closure models for stably-stratified geophysical flows. *Boundary-Layer Meteorology*, 146:341–373, 2013.